Chapter 2. Physical Properties of Sea Ice Relevant to Remote Sensing

W. B. TUCKER III, DONALD K. PEROVICH, AND ANTHONY J. GOW
Cold Regions Research and Engineering Laboratory, 72 Lyme Road, Hanover, New Hampshire 03755-1290

WILFORD F. WEEKS
Alaska SAR Facility, Geophysical Institute, University of Alaska, Fairbanks, Alaska 99775-0800

MARK R. DRINKWATER
Jet Propulsion Laboratory, California Institute of Technology, 4800 Oak Grove Drive, Pasadena, California 91109

An understanding of the physical processes and properties of sea ice is critical in interpreting microwave signatures. The incorporation of salt in the form of brine inclusions in the ice makes sea ice a vastly different material than freshwater ice. The amount of brine incorporated is largely growth-rate dependent. In columnar ice brine is trapped in inclusions within ice crystals in a platelet substructure, while in frazil ice the inclusions are located between the crystal boundaries. Brine drainage begins immediately after ice formation, occurring slowly during the growth season, but increasing considerably during summer. In the Arctic, enhanced surface melting, coupled with increased interconnectivity of the brine inclusions, almost completely flushes the salt from the ice in the upper layers, leaving air voids and channels; a process that greatly increases the ice's porosity.

The crystal texture of the upper meter of the ice also shows the effects of protracted warming, with rounding of crystal boundaries and virtual elimination of the brine platelet substructure. Such effects are not evident in Antarctic sea ice where pronounced surface melting apparently does not occur, resulting in an absence of both surface melt ponds and the melt-pond–hummock relief so characteristic of similar floes in the Arctic.

Pressure ridges are evident in both polar regions, although they are larger and more numerous in the Arctic. Small-scale surface properties, such as ice surface roughness, are very important to microwave remote sensing. Frost flowers and snow on recently formed ice absorb brine, greatly affecting the surface dielectric properties. Excessive snow cover can depress both multiyear and first-year floes sufficiently to cause sea water to flood the surface, resulting in the misidentification of ice types in microwave algorithms.

Microwave Remote Sensing of Sea Ice
Geophysical Monograph 68

2.1 INTRODUCTION

Remote sensing in the polar regions has significantly increased our understanding of sea ice extent and variability. The capability of all-weather day and night surveillance of the ice packs has both enhanced research capabilities and helped to accomplish operational objectives. For instance, continuous monitoring of the ice extent and concentration, facts that are routinely available from satellite passive microwave systems, is proving invaluable to scientific investigations involving sea ice climatology. This capability has also improved navigation and assisted petroleum development operations. Other useful products, such as the automated characterization of ice types and velocities, are currently being developed. In addition, field studies associated with these remote sensing developments have contributed to our understanding of the physical properties of the ice.

Early sea-ice remote-sensing experiments consisted of aircraft missions that carried sensors designed for either land, oceanic, or atmospheric applications. Microwave sensors have evolved considerably since those early missions, and some are now designed with sea ice as one of the primary media of interest. Both active and passive microwave sensors play major roles in these missions. Useful geophysical products can be derived from each type of sensor by using a range of frequencies, polarizations, and look angles. Ice properties exhibit tremendous variability in both vertical and horizontal dimensions. Ice types can range from essentially freshwater ice in refrozen melt ponds to very saline new ice to extremely porous ancient multiyear ice.

In this chapter, we address the sea ice properties that are important to microwave remote sensing. For passive microwave measurements, the ice's emissivity is the electromagnetic characteristic of interest. Emissivity is a function of the effective surface reflectance and of both surface and volume scattering. The reflectivity depends upon the bulk dielectric properties, which are functions of the distribution of the brine, air, and solid salt within the ice. Scattering

depends upon the surface roughness and inhomogeneities within the ice, as well as the bulk dielectric constant. Active microwave instruments measure the backscatter, which is dominated by surface and volume scattering. Again, roughness and spatial variations in the dielectric properties contribute to the magnitude of the scattering.

Physical properties of the ice that will be discussed are the crystal structure, brine and air content, and surface properties. The properties and evolution of both first-year and multiyear ice, defined here as ice that has survived one or more summers, are described. This description of ice properties and processes is intended to set the stage for the chapters that follow, describing the nature of microwave–sea-ice interactions in some detail.

2.2 FIRST-YEAR ICE

2.2.1 Growth of First-Year Ice

The freezing of seawater differs from that of freshwater in two ways due to the inclusion of salt. First, salt depresses the freezing point of water (in degrees Centigrade) according to the approximation $T_f = -0.003 - 0.0527 S_w - 0.00004 S_w^2$ [Neumann and Pierson, 1966], where S_w is the salinity of the water in parts per thousand. Second, the temperature of the maximum density of seawater for salinities greater than 24.7‰ is less than the freezing point. The result is that continued cooling of seawater in this salinity range results in an unstable vertical density distribution. This leads to convective overturning that continues until the water reaches the freezing point. Because of the oceanic density structure, this convection is limited to a relatively shallow layer. This well mixed layer, which presumably ranges from 10- to 40-m thick [Doronin and Kheisin, 1975], must cool to the freezing point before freezing can begin. Subsequent brine rejection by the growing ice causes additional convective overturning that can further deepen the mixed layer.

Initial ice formation begins at the water surface, where the heat loss is greatest, providing the small amount of supercooling necessary for ice growth. Ice growth begins with the formation of small platelets and needles, called frazil. As frazil crystals continue forming, a soupy mixture of unconsolidated crystals and seawater is created, commonly referred to as grease ice. With continued freezing under quiet conditions, the frazil crystals begin to coalesce, freezing together to form a solid cover up to 10-cm thick. This thin cover, which behaves elastically, is called nilas. Often, however, the action of wind and waves influences the configuration of the solid cover that forms. In leads, wind frequently herds the frazil to the downwind side, forming accumulations that can reach 1 m in thickness. Wind-driven circulation in leads can also cause frazil to accumulate in bands. In large open areas, such as occur in the marginal ice zones of the Arctic and Antarctic, wind and wave action cause the formation of pancake ice, which consists of circular masses of semiconsolidated frazil. Pancakes commonly grow to diameters of 0.3 to 3.0 m, and in many cases develop several-centimeter-high raised rims from bumping together and from sloshing of newly formed crystals onto existing pancakes. The slush forming in the open areas between the pancakes eventually consolidates to form either a solid field of pancakes or a combination of pancake and sheet ice. In the Antarctic, the rafting of pancake ice is thought to be largely responsible for the thick masses of ice with a frazil texture. Such ice floes have been extensively observed in the Weddell Sea [Lange et al., 1989].

An important aspect of the occurrence of frazil is that it forms the initial ice cover and, once it has consolidated, insulates the underlying ocean from the cold atmosphere. Further growth of ice must take place beneath this initial skim. Most often, this occurs as congelation growth, which is the freezing of seawater directly to the bottom of the existing sheet as the result of heat conduction upward through the overlying ice. In these cases, the growth rate is determined by the temperature gradient in the existing sheet and its effective thermal conductivity.

Once the ice sheet forms, the crystals at the ice–water interface lose one degree of growth freedom. As a result, noncompetitive crystal growth can only occur when the grain boundaries are exactly perpendicular to the freezing interface. Through a process referred to as geometric selection, crystals in unfavored orientations are eliminated by crystals oriented in the favored growth direction. This selection process occurs in a transition layer that is usually 5- to 10-cm thick [Weeks and Ackley, 1986]. The final crystal structure that develops contains vertically elongated columnar crystals aligned parallel to the direction of heat flow and having their c-axes oriented generally parallel to the ice–water interface.

2.2.2 Crystal Structure

Exclusive of the effects of snow cover, typical Arctic sea ice consists texturally of three layers resulting from the conditions during growth described above. The first two layers are generally relatively thin and consist of the initial frazil layer underlain by the transition layer. Columnar ice generally comprises the remainder of the ice sheet. There are, however, ample exceptions to this typical structure. Large accumulations of frazil-textured ice have been reported in Antarctic sea ice [Gow et al., 1987a; Lange et al., 1989], and significant amounts of frazil have been observed in samples from the marginal ice zones of the Arctic. Mixtures of the two crystal types are also not uncommon.

The elongated crystals characteristic of columnar ice contain a predominant crystal substructure. Within each grain, pure ice plates are separated by parallel layers of brine inclusions. These inclusions are the result of constitutional supercooling that allows the systematic entrapment of brine. Constitutional supercooling is caused by the more rapid diffusion of heat than salt at the freezing interface, resulting in a supercooled condition in the fluid ahead of the interface. As a result a nonplanar, dendritic interface develops with the associated entrapment of brine between dendritic plates, which are composed of pure ice.

This aggregation of plates at the base of the sea ice sheet is called the skeleton layer and is generally 1- to 3-cm thick (Figure 2-1). The spacing between the plates ranges from a few tenths to about 1 mm, and is largely a function of the growth rate [Lofgren and Weeks, 1969; Nakawo and Sinha, 1984]. Therefore, each columnar ice crystal contains a number of brine inclusions located in the grooves between the pure ice plates. Figure 2-2 shows a horizontal thin-section photograph depicting the ice-plate–brine-inclusion substructure within individual crystals of sea ice. The salinity of the ice sheet is ultimately determined by the abundance of brine inclusions and the amount of solid salt and brine within the inclusions.

The grain size of these columnar crystals varies considerably. The horizontal diameter of the crystals can be a few tenths to several centimeters, while the vertical length of the crystals can be tens of centimeters. Crystal sizes generally increase with depth [Weeks and Hamilton, 1962; Paige, 1966]. Typical diameters range from 0.5 cm near the top of the sheet to 2 to 3 cm near the bottom of the sheet.

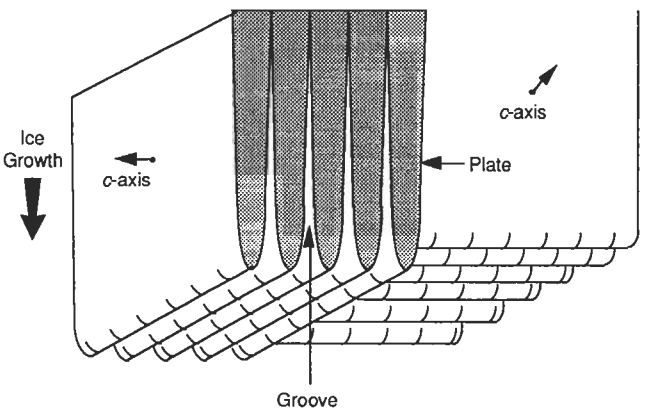

Fig. 2-1. Dendrite and groove structure of two columnar sea ice crystals. Residual brine is trapped in grooves between dendrites (plates), which remain essentially salt free.

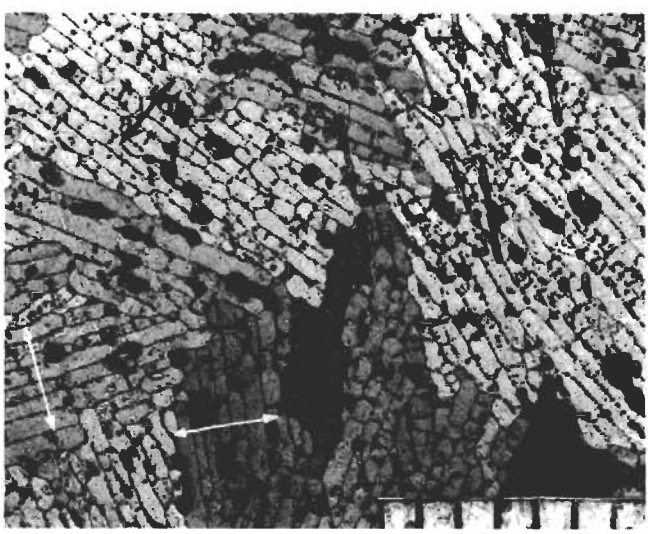

Fig. 2-2. Horizontal cross-section of a thin section of sea ice showing multiplate and brine layer substructure of individual crystals. Arrow indicates *c*-axis orientation in three of the crystals. Scale subdivisions measure 1 mm.

As noted, typical congelation growth results in columnar crystals that have their *c*-axes oriented substantially in the horizontal plane. The *c*-axes are normal to the dendritic plates (Figure 2-1). In some cases, the crystals show no preferred alignment within the horizontal plane. However, strong alignments in this plane are quite common. Weeks and Gow [1978, 1980], Langhorne [1983], Langhorne and Robinson [1986], and Stander and Michel [1989] found that the direction of preferred *c*-axis alignment was coincident with the direct of current motion at the ice–water interface. It is hypothesized that crystal growth is enhanced in this direction by more effective removal of the solute buildup at the growing interface by increased turbulence. Of significance to remote sensing is that the preferred alignment of the *c*-axes has been found to polarize signals of impulse radar systems [Campbell and Orange, 1974; Kovacs and Morey, 1978]. Using a radar with a center frequency of 625 MHz, which is typically used to determine ice thickness, no bottom reflection was obtained when the radar antenna E-field was oriented normal to the alignment of the *c*-axes in first-year fast ice. Observations indicate that aligned *c*-axes can develop in the bulk of the congelation component of first-year ice [Weeks and Gow, 1978, 1980] and that such alignments may extend over areas of many tens of square kilometers [Cherepanov, 1971; Weeks and Gow, 1978].

Although we have thus far concentrated almost entirely on columnar ice, granular ice can also be an important constituent of the ice cover. As mentioned earlier, the initial consolidated skim usually consists of granular ice. Snow ice, another form of granular ice, may also form on the ice surface. This ice type results from the freezing of the snow cover that has become saturated with water whose source may be seawater, rainwater, or meltwater. Snow ice can generally be distinguished from other granular ice types because it is somewhat coarser grained and contains more air bubbles. Such ice can be fresh or saline depending on the conditions of saturation.

Frazil ice may also be observed at some depth in the ice sheet. Under certain circumstances, frazil is believed to form at depth in the water column and aggregate onto the bottom of the ice sheet. The large amounts of frazil observed in the Weddell Sea of Antarctica may form in this manner [Gow et al., 1982, 1987a]. The rafting of pancake ice, which is extensive in the Weddell Sea, may also be responsible for enhancing frazil ice thickness [Wadhams et al., 1987; Lange et al., 1989]. In the Arctic, the occurrence of frazil appears to be much more restricted. Most often it appears to be associated with turbulent hydrodynamic conditions associated with the earliest stages of ice growth. Granular ice and mixed columnar and granular ice have also been observed in substantial proportions in cores obtained from ridges [Tucker et al., 1987]. In this case, frazil is believed to originate in the voids between the blocks of ice incorporated when the ridge was formed. It has also been found on

the flanks and keels of ridges [Tucker et al., 1987], suggesting that freely suspended frazil crystals in the water column are collected by the ridge as it moves relative to the seawater. The crystals then accumulate on the sides of ridge keels, where they eventually consolidate. Lange and Eicken [1991b] believe that deformation processes can cause frazil ice to be incorporated both between and beneath columnar ice sections.

Granular ice occurs in a wide variety of crystal sizes. Snow ice has crystal sizes ranging from 3 to 5 mm. Nilas, the thin ice cover resulting from the consolidation of grease ice, can have grains as small as a few tenths of a millimeter up to 2 mm. Likewise, pancake ice typically has small grains, measuring a few millimeters or less. Frazil crystals found deep within the ice sheet range from millimeters to several centimeters in diameter. In many cases fine-grained columnar crystals may be confused with granular ice, particularly in a horizontal thin section. Usually, however, the brine platelet substructure is sufficient to distinguish between the two types of ice.

2.2.3 Incorporation of Brine and Air

The incorporation of salt and air into the ice sheet is extremely important with regard to remote sensing in that the electromagnetic properties of the sheet, including the dielectric constant, the reflectivity, and volume and surface scattering, are heavily dependent on the distribution of liquid brine and gas within the ice. Also crucial to remote sensing is that the incorporation of brine gives rise to strong vertical anisotropy in a congelation ice sheet. This unique structure results from the extended columnar crystals, the vertical elongation of brine pockets, and the vertical orientation of brine drainage systems.

The temperature regime in the ice, both at the time of observation and at the time of initial formation of each layer, controls many of the characteristics of the sheet. The brine inclusion process is temperature dependent in that the plate spacing is almost solely determined by the growth rate. With more rapid freezing, the plate spacing is narrower and more brine is entrapped, resulting in higher salinities. The amount of entrapped salt is correspondingly less at lower growth rates. The plate spacing has been found to be generally inversely proportional to the square root of the growth rate [Weeks and Ackley, 1986]. Brine is also entrapped as pockets in consolidated granular ice. However, as these crystals do not have the characteristic substructure, the inclusions are found along grain boundaries and at the intersections of grains.

The amount of salt entrapped as brine in the ice also depends on the salinity of the water. Laboratory measurements by Weeks and Lofgren [1967] and Cox and Weeks [1975, 1988] indicate that the relationship between the initial salinity of the ice (S_i) and the salinity of the water from which the ice formed (S_w) can be expressed as $S_i = K_{eff}S_w$, where K_{eff} is the effective distribution coefficient, which is growth-rate dependent.

The amount of liquid brine in the ice sheet at any time after initial entrapment is dictated by the requirements of phase equilibrium [Weeks and Ackley, 1986], which fix the salinity of the brine that coexists with ice at a given temperature. That is, changes in the temperature of the ice will be accompanied by changes in the size of the brine pockets resulting from freezing or melting on the walls of the pockets until the salinity of the brine reaches the new equilibrium composition. The result is that, due to temperature changes, constantly varying proportions of brine, air, and ice exist in the brine inclusions so that the brine salinity at every level in the ice sheet is exactly the equilibrium value at that temperature.

Because the most rapid freezing invariably occurs at the top of the ice sheet, it might be assumed that the highest salinities would be found there. Although this is generally true, it must be noted that the process of brine drainage begins immediately after initial entrapment. The dominant mechanisms for brine loss from growing ice sheets are gravity drainage and brine expulsion. Brine expulsion results from pressure increases in the brine pockets due to freezing. Any decrease in the temperature of the ice will cause ice to form on the walls of the brine cavities, thereby increasing the salinity of the remaining brine to maintain phase equilibrium. Since the new ice on the cavity wall has about a 10% greater volume than the water from which it froze, some brine is expelled through cracks around the pocket caused by the pressure increase associated with the volume change. While most of the expelled brine would be expected to drain downward into the warmer and therefore more porous underlying ice, in thin ice, brine is also expelled upward onto the ice surface. This produces a thin layer of highly concentrated brine on the surface of the ice [Martin, 1979]. This process appears to be enhanced by capillary effects leading to the "wicking up" of brine by snow and frost flowers [Drinkwater and Crocker, 1988]. Present data suggest that brine expulsion is primarily of importance in the upper layers of sea ice sheets.

The major desalination mechanism of a growing ice sheet is gravity drainage. Because the top of the ice is colder, the brine higher in the ice sheet is denser and will drain downward. This effect is enhanced by a downward increase in the permeability of the ice. The formation of brine channels, vertical tubes centimeters to tens of centimeters long created by the interconnection of brine pockets, appears to be particularly important in increasing permeability. Although some aspects of the formation and behavior of these features are well understood [Eide and Martin, 1975; Lake and Lewis, 1970], many of the details have, as yet, not been thoroughly investigated. As a result of the continuing desalination process, the bulk salinity of the ice sheet decreases as it thickens and ages. This effect is demonstrated by the idealized profiles shown in Figure 2-3. These show the typical C-shaped profiles found in growing first-year ice. The upper portion of the ice has a higher salinity because it initially entraps more salt as a result of its more rapid growth rate. The high salinities in the lower portion of the ice result from the fact that although the

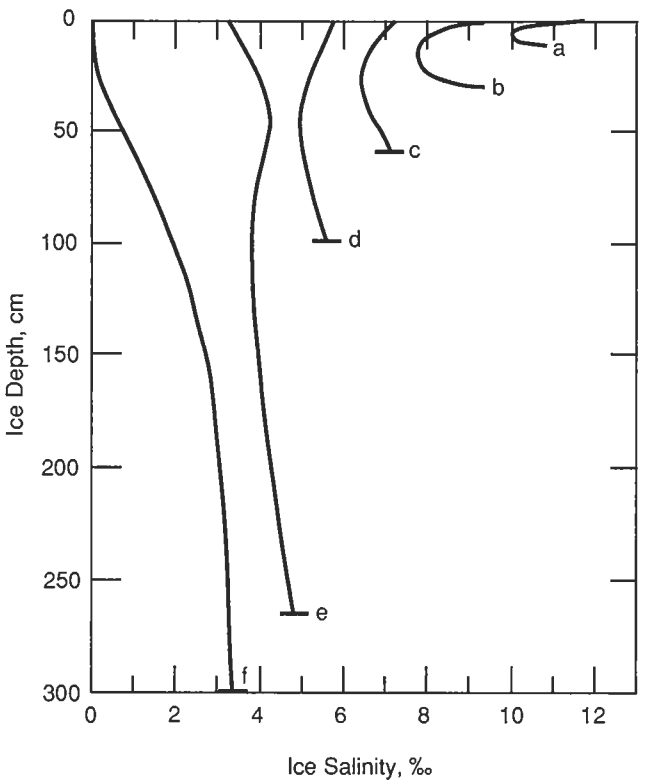

Fig. 2-3. Idealized salinity profiles in Arctic sea ice of various thicknesses. Curves (a) through (d) represent changes observed in first-year ice. The remaining curves are for two types of profiles found in multiyear ice. Curve (e) typifies the salinity distribution beneath low areas where the surface is close to the freeboard level, while curve (f) represents the salinity profile beneath hummocks and other elevated areas. (Reprinted with permission from Maykut [1985]. Copyright CRC Press, Inc.)

initial salt entrapment in this ice is commonly less than in the overlying ice, because this ice has just formed, it has lost little brine. Also, the lower layers of the ice receive brine that has drained from above. At mid-levels, slower growth rates and sufficient time to allow drainage to begin combine to produce lower salinities. These effects also act to reduce the bulk salinities as the ice becomes thicker.

The desalination process results in small-scale variations in salinity. For example, Weeks and Lee [1962], Tucker et al. [1984a], and Eicken et al. [1991] demonstrated that salinity profiles of cores taken within 1.0 m of each other from the same ice sheet can be significantly different. They observed salinities of the upper 10 cm differing by as much as 2‰ for ice that was structurally identical. These variations were attributed to the location of vertical brine drainage channels, with ice in the vicinity of a drainage channel being less saline.

Gas (air) is also entrapped in the ice as it forms. The gas volume subsequently increases as brine drainage takes place, leaving empty cavities and drainage channels. As might be expected, the volume of gas trapped at initial freezing is quite small, generally ranging from 0‰ to 15‰. Air volumes increase significantly as drainage occurs, vacating the brine cavities. Total porosities (air plus brine) can reach 200‰, particularly at the bottom of the ice sheet. More often, measured total porosities are found to be 20‰ to 60‰. Normally densities of first-year ice are about 0.91 to 0.92 mg/m^3, with a full range from 0.89 to 0.925 mg/m^3 [Cold Regions Research and Engineering Laboratory (CRREL), unpublished document, Hanover, New Hampshire].

2.2.4 Polar Contrasts

The differences in the properties of Arctic and Antarctic first-year ice exist because of the very different growth conditions that are directly related to contrasts in the land and sea relationships in the two polar regions. The Antarctic continent lies substantially poleward of 70° S, and sea ice forms from the coast outwards. In general, ice that forms in the south is advected generally northward, where it melts [Ackley and Holt, 1984]. Therefore, Antarctic sea ice essentially constitutes a marginal ice zone that undergoes very large changes in ice extent and whose northward progression is hindered by the warmer ocean, warmer atmosphere, and ocean swell. The Arctic, on the other hand, contains an ocean basin surrounded by land. The ice extent here undergoes less seasonal change than in the Antarctic and much less ice is advected from the basin because there are few passages through which ice can exit the basin. Also, the land-locked nature of the basin plus the large amount of multiyear ice that survives the summer combine to limit the effective open water fetch at the southern limits of the pack. As a result, both wave effects and the contribution of frazil ice are less in the Arctic than in the Antarctic.

Besides major differences in the ice extent and concentration, profound differences exist between ice thicknesses in the two regions. First-year ice thickness in the Antarctic varies greatly with location, measuring on the order of 0.50 to 0.75 m in parts of the Weddell Sea [Wadhams et al., 1987; Lange and Eicken, 1991a] to as much as 3 m in coastal embayments, where air temperatures are colder and the oceanic heat flux is negligible or in some cases even negative. In the Arctic, it is not uncommon to have first-year ice in excess of 1 m, frequently reaching 2 m [Bilello, 1980], though ice in the peripheral seas of the Arctic is substantially thinner. For example, in the Bering and Labrador Seas, where air temperatures are more moderate than in the Arctic Basin, thicknesses of undeformed ice seldom exceed 1.0 m. However, rafting occurs frequently in the thin ice of these areas, increasing the mean thicknesses to 1.25 to 1.50 m [Drinkwater and Squire, 1989; Carsey et al., 1989].

Major differences are apparent in the crystal structures of Arctic and Antarctic ice. In the Antarctic, far more frazil or granular ice has been observed than in the Arctic. Recent studies of Arctic Basin sea ice have reported granular ice contents of undeformed ice to be about 10% to 15% [Gow et al., 1987b]. In contrast, ice sampled in the Weddell Sea contained about 50% to 60% frazil ice. Recent investigations by Jeffries and W. F. Weeks [unpublished data] confirm that frazil is also an important component of sea ice

in the Western Ross Sea. Figure 2-4 compares the granular and columnar contents of recent measurements made in the Arctic and Antarctic. A contributing factor to the widespread occurrence of frazil in the Antarctic is increased wind and wave turbulence, which enhances frazil production. Associated with these more dynamic conditions is the rafting of frazil-rich pancake ice and ice sheets. Platelet ice, which consists of large plate- and wafer-like crystals, has also been observed in the Antarctic [Gow et al., 1987a; Dieckmann et al., 1986; Lange et al., 1988]. This type of ice has yet to be identified in the Arctic. Unfortunately, other large areas of Antarctic sea ice remain virtually unstudied. Thus, extrapolation from the Weddell Sea regarding structure and other physical characteristics could lead to errors.

The amount of multiyear ice also differs between the Arctic and Antarctic. Because Antarctic ice is so efficiently advected from the coastal regions north to the marginal areas where it melts, multiyear ice appears to be scarce around most of Antarctica. Large oceanic heat fluxes efficiently melt the thin first-year ice. Ice in the Antarctic regions does not appear to last longer than 1 to 2 years [Gow and Tucker, 1990], except in isolated bays where fast ice may remain in place for several years. In sharp contrast, Koerner [1973] found that multiyear ice in the Arctic comprised at least 70% of the ice cover during a surface transect of the Central Arctic. Comiso [1990] also found large concentrations of Arctic multiyear ice using passive microwave data. Stochastic model studies by Colony and Thorndike [1985] indicated that ice-floe residence times of 5 to 7 years in the Arctic Basin are not unusual.

Antarctic first-year ice appears to be only slightly more saline (0.3‰ to 0.5‰) than its Arctic counterpart [Gow and Tucker, 1990]. The higher Antarctic salinities probably result from more rapid growth rates associated with generally colder temperatures. It may also be possible that more brine is retained in consolidated frazil because its structure impedes the development of brine drainage mechanisms. Gow et al. [1987a] found no compelling evidence that such was the case for the sea ice they examined in the Weddell Sea. To date, observations do not verify this hypothesis.

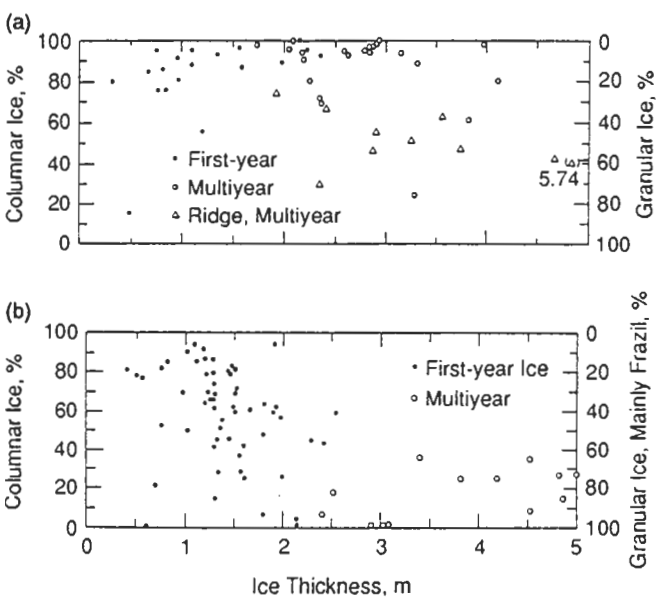

Fig. 2-4. Percentage of columnar and granular ice versus ice thickness in floes from (a) the Fram Strait [Gow et al., 1987b] and (b) the Weddell Sea [Gow et al., 1987a].

2.3 EVOLUTION OF MULTIYEAR ICE

2.3.1 Desalination

Ice undergoes dramatic changes during the melt season. The most obvious change is the large decrease in salinity. This desalination occurs primarily in response to temperature changes within the ice. Since the largest increases in temperature occur near the surface, the greatest desalination is also observed in the upper layers of the ice. Two effects are important in decreasing the salinity. First, the warming causes significant changes in the brine inclusions. As temperatures rise, ice goes into solution in the brine to produce the new lower equilibrium salinities. Associated with this brine volume increase, the brine pockets enlarge and tend to coalesce into vertical channels that facilitate gravity drainage of the brine and desalination of the ice. Martin [1979] showed photographic evidence of these channels.

In the Arctic, the improved system of brine drainage is further enhanced by the second major effect of summer—flushing of the ice with surface meltwater. Melting snow and ice provide a source of fresh water that can percolate through the ice, greatly reducing the salinity of the upper 50 to 100 cm. The largest changes occur during the late spring and early summer, when significant melting of the snow cover takes place. Salinities of the upper 50 to 100 cm are reduced to less than 1‰, down from previous values of 4‰ to 7‰. Although desalination occurs in Antarctic sea ice as it ages, the desalination is much less than in the Arctic, mainly because surface melting is uncommon [Andreas and Ackley, 1982]; the snow cover remains intact, melt ponds do not form, and albedos remain high. Therefore, in the Southern Hemisphere, flushing is not an important mechanism in draining brine from the ice.

Plots of bulk ice salinities versus thickness for Arctic and Antarctic sea ice are shown in Figure 2-5. For Arctic first-year ice there is a substantial decrease in salinity with thickness due to less entrapment as the growth rate decreases. Brine drainage activity is probably also manifested in the decreased salinities of thicker (1 to 2 m) first-year ice. The salinities of the thicker multiyear ice also decrease with increasing thickness, although the gradient is much less. The overall bulk salinity of Arctic multiyear ice is 3‰ to 4‰. Comparison of Figures 2-5(a) and (b) indicates that Antarctic ice has slightly higher salinities than Arctic ice of comparable thickness and does not appear to be as strongly dependent on thickness. Certainly the absence of flushing contributes to higher salinities in the Antarctic ice.

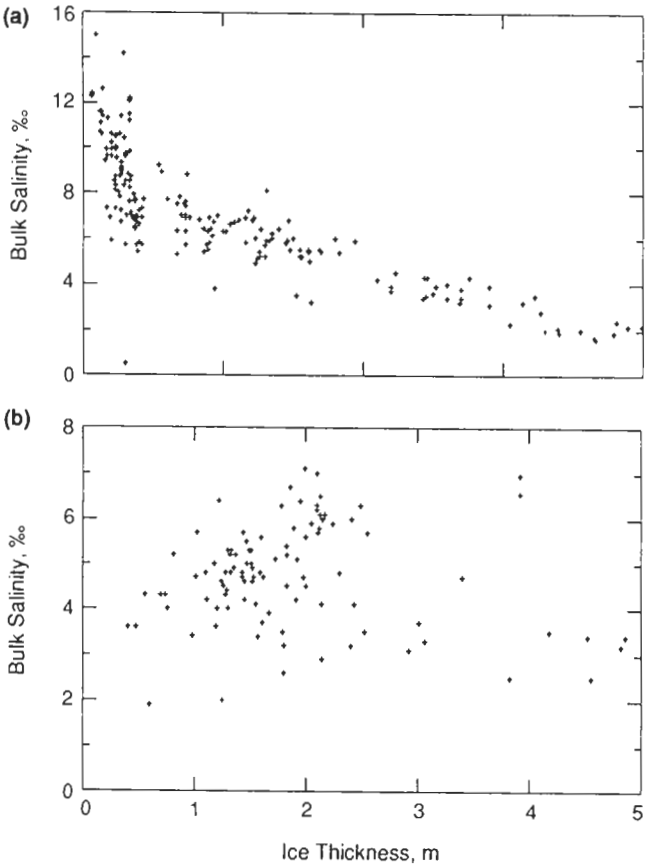

Fig. 2-5. Scattergrams of the bulk ice salinity versus ice thickness for (a) Arctic sea ice during the growth season and (b) Antarctic sea ice. The data were obtained from a variety of published and unpublished sources.

2.3.2 Crystal Retexturing

The crystalline texture of the ice is also affected by the summer melt cycle. This effect appears especially true of Arctic ice, which is apparently enhanced by the protracted warming and melting of the ice surface. In effect, the warming causes the retexturing of the crystals. The originally sharp crystal boundaries become rounded and the well-defined brine platelet layer structure is substantially modified or even eliminated. Figure 2-6 shows an example of this retexturing. The depth of the retexturing may exceed 100 cm. While still columnar in texture, the remaining structure bears little resemblance to that of the original ice. It is brine poor with salinities near zero, and glacial-like in appearance. Such thermally activated retexturing has to date not been reported in Antarctic multiyear ice.

2.3.3 Formation and Modification of the Surface Layer

In the previous two sections, we have described effects that modify the properties of the ice on its way to becoming multiyear ice. These changes are most pronounced in the uppermost layers of the ice, primarily the top meter, the portion of the ice that is most important to high-frequency remote-sensing instruments [Tucker et al., 1991]. The two major changes are the large reduction in salinity and crystal retexturing. These alterations combine to produce ice with properties that resemble those of freshwater ice.

Another major effect is an increase in porosity of the upper layers of the ice. As the brine drains from the upper layers of the ice, the air volume in the upper 10 to 30 cm of the multiyear ice is greatly increased. This is accompanied by a decrease in density, to values as low as 0.6 mg/m^3 [CRREL, unpublished data, Hanover, New Hampshire]. Higher porosities and lower densities appear to be especially likely on weathered ridges where the increased absorption of solar radiation may play a large role. There is also less snow to melt off of the ridge peaks. The decrease in salinity is also greater in elevated, drained areas as opposed to the ice at or below sea level.

Other modifications of the surface include the effects of fresh water or snow saturated with water freezing on the surface. Occasionally, layers of fresh ice have been observed on the surface of multiyear ice [Tucker et al., 1987]. This effect might be expected if only part of the snow melted off, but, in the Arctic, melting of the snow cover is usually quite complete. We expect that this formation of a fresh ice layer occurs in late summer or fall from rain that freezes on the surface or recent snow that melts and refreezes. This effect as well as the increased porosities discussed above is not observed in Antarctic sea ice.

In the Fram Strait region of the Eastern Arctic, the surfaces of multiyear floes can be flooded with seawater. Snow covers in this region are thicker than those observed in the Western Arctic [Tucker et al., 1987]. On some floes, the snow becomes deep enough to depress the floe and cause surface flooding. In late spring, this was observed on roughly 30% of the floes sampled in the Fram Strait [Perovich et al., 1988]. The seawater then infiltrates the upper layers of the multiyear ice creating a high salinity. Microwave signatures from this flooded ice can easily be confused for first-year ice [Tucker et al., 1991], with consequent errors in the estimation of multiyear ice concentrations [Comiso, 1990]. Such flooding has been observed in the Antarctic on both first-year and multiyear ice [Lange et al., 1990; Wadhams et al., 1987].

2.3.4 Melt Ponds and Hummocks

Melt ponds are a significant feature of Arctic multiyear sea ice. In fact, the characteristic appearance of multiyear ice largely results from the presence of melt ponds. The surface of multiyear ice has a characteristic hummocky appearance produced by alternating low refrozen melt ponds and adjacent hummocks. Small hummocks may have originally been level ice, whereas larger hummocks probably are weathered remnants of deformed ice.

In early summer, meltwater covers a large percentage of the surface of the floe as a result of snow melting on the level ice surface. When the melt cycle becomes more advanced, the coverage of the surface by melt ponds will be reduced to

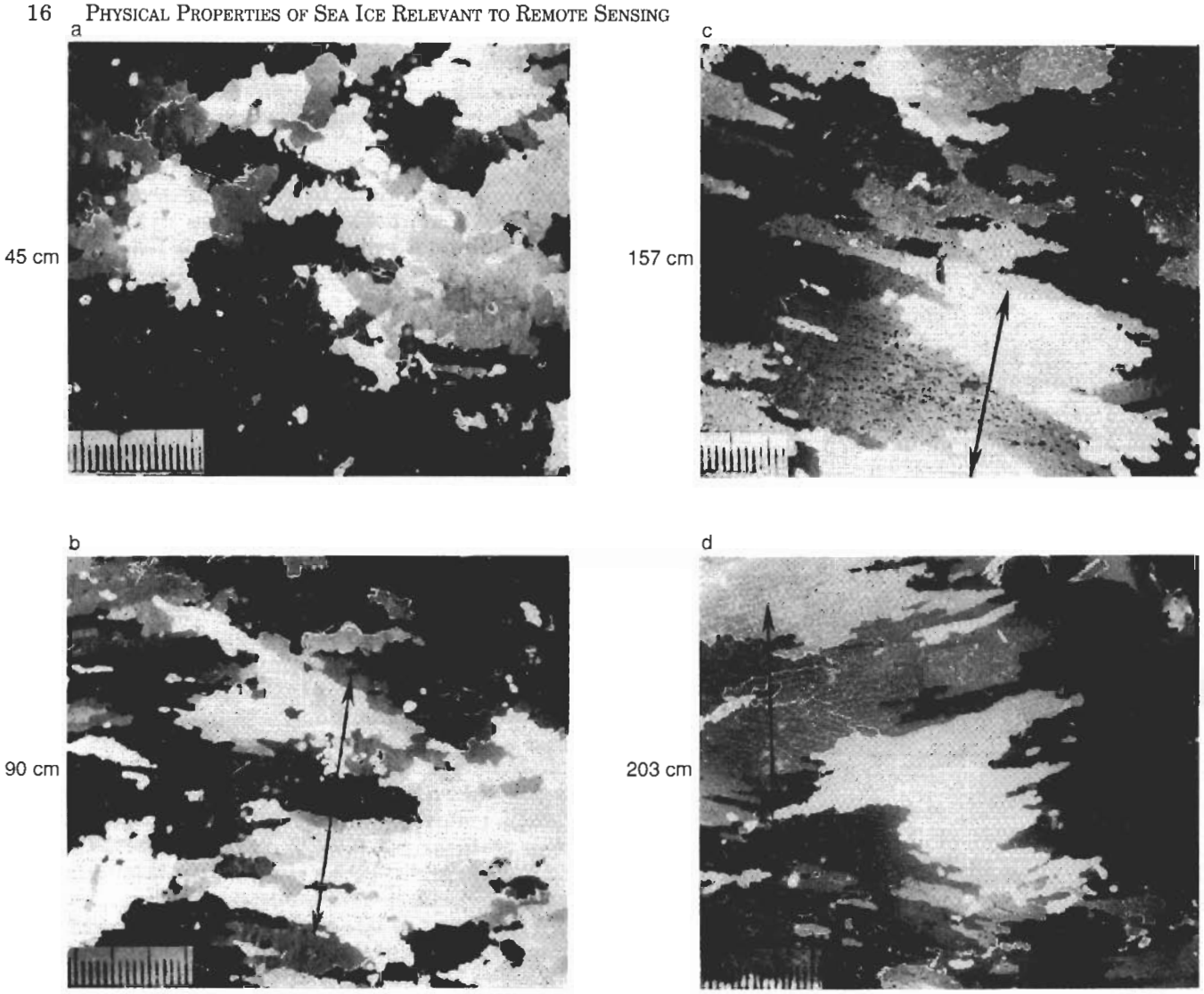

Fig. 2-6. Horizontal thin sections demonstrating retexturing of ice in the upper layers of an Arctic multiyear floe for (a) 45 cm, (b) 90 cm, (c) 157 cm, and (d) 203 cm. Notice that in (b) the original *c*-axis alignment (arrowed) is still preserved despite nearly complete loss of brine pocket substructures, in contrast to substructure still maintained in deeper unretextured ice [Gow et al., 1987b]. Small-scale subdivisions measure 1 mm.

about 30% [Maykut, 1985]. Surface drainage into adjacent leads is also effective in reducing aerial coverage. The melt ponds decrease the surface albedo and absorb more radiation, gradually deepening and decreasing the area of surface coverage. Ponds are commonly 50 cm to 1-m deep. They occasionally melt completely through a floe, in which case the pond may subsequently become filled with seawater. When such ponds freeze, they produce ice with essentially first-year characteristics.

Ponds begin to freeze during the late summer and early fall. At this time approximately 10% to 30% of the ice's surface is covered by ponds. With the exception just mentioned, refrozen melt ponds consist of fresh ice very similar to lake ice. A core through a pond nearly 1-m thick underlain by retextured columnar ice is shown in Figure 2-7. The top of this core profile shows the zero salinity characteristic of fresh pond ice. Another interesting structural feature of the pond ice is the very coarse-grained nature of the crystals exhibiting substantially vertical *c*-axes. This is a feature often observed in lake ice [Gow, 1986]. Grain sizes in melt ponds can range from very small (millimeter) to quite large (several centimeters). The melt pond ice often contains long tubular bubbles a few millimeters in diameter, but tens of centimeters long. Densities of melt pond ice range from 0.85 to 0.92 mg/m^3, depending upon the amount of air entrapped. Air volumes can be as large as 80‰ to 90‰ in the case of ice containing a high concentration of bubbles, but more often are 20‰ to 40‰ [CRREL, unpublished data, Hanover, New Hampshire].

Melt ponds are uncommon in the Antarctic because the extensive surface melting common to the Arctic seldom occurs. Andreas and Ackley [1982] speculated that lower relative humidities and stronger winds enhance turbulent heat losses. Under these conditions, surface melting will

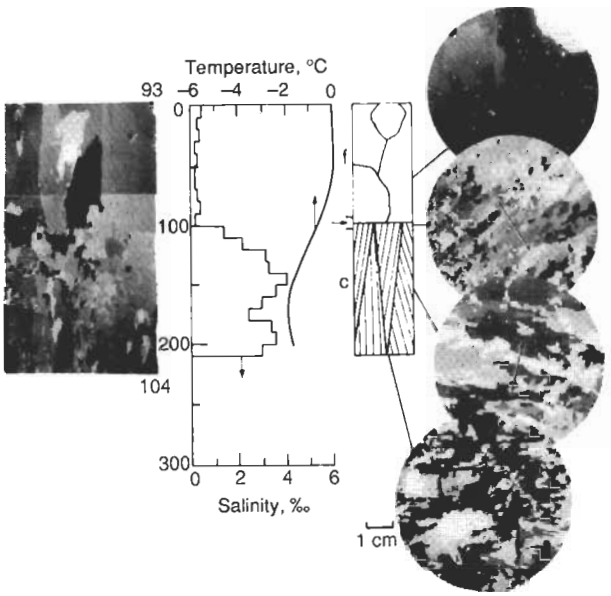

Fig. 2-7. Salinity, temperature, and structure profiles from a ponded multiyear ice floe in the Fram Strait. The vertical thin section shows the transition between the ponded and columnar ice at around 100 cm in depth. The *c*-axis alignments in horizontal thin sections are indicated by arrows [Gow et al., 1987b].

only occur when the air temperature is significantly above 0°C, a situation only rarely observed in the Antarctic.

Hummocks also have low salinities because their raised relief enhances brine drainage during summer. The upper 10 to 20 cm in particular may retain very little brine. An example of a core profile from a hummock on a floe composed entirely of columnar ice is shown in Figure 2-8. The density of the upper 10 cm is quite low, caused mainly by the presence of evacuated brine channels with some additional porosity due to melting enhanced by the absorption of shortwave radiation. The air volume is very large (300‰) for the upper 10 cm. As expected, salinities are very low. It is often difficult to obtain accurate quantitative measurements of density for the near-surface ice of multiyear hummocks and ridges because of the brittle degraded nature of the ice.

On mid-relief ice (areas between melt ponds and hummocks), upper layer salinities are also quite low, often close to zero. Densities are also low, typically 0.75 to 0.85 mg/m^3, although they are not as low as the near surface of the well-drained hummocks. Air volumes in the upper layers range from 80‰ to 95‰, decreasing with depth to 5‰ to 25‰. Likewise, densities and salinities increase with depth.

2.3.5 Properties of Multiyear Versus First-Year Ice

In comparing multiyear and first-year ice properties, it is useful to consider the Arctic and Antarctic separately, since the ice properties are so different in these two areas.

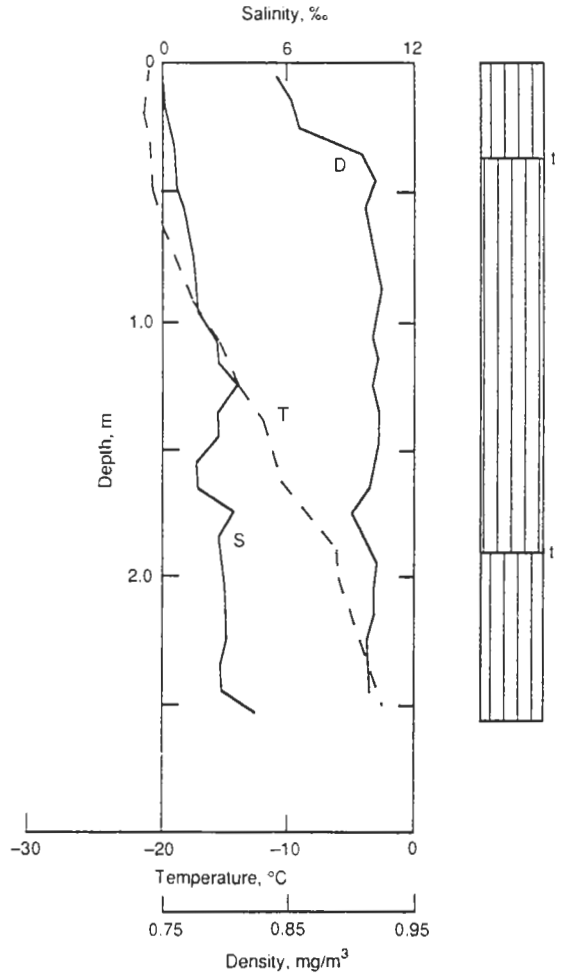

Fig. 2-8. Salinity (S), temperature (T), and density (D) profiles from an ice core drilled through a hummock on a multiyear floe. The ice at this location on the floe consisted entirely of columnar ice, with Tr referring to an obvious transition [A. J. Gow, CRREL, unpublished data, Hanover, New Hampshire].

The Arctic shall be addressed first, since the greater variability in properties occurs there. Large differences are apparent in the thickness and appearance of first-year and multiyear ice. Arctic first-year ice grows to a maximum thickness of about 2.0 m in its single season. The equilibrium thickness of undeformed multiyear ice is 3.0 to 4.0 m [Maykut and Untersteiner, 1971], though the thickness of multiyear ice varies greatly. On a single floe, its thickness may range from less than a meter to tens of meters. The thinner ice results from pronounced ablation during the summer, probably beneath a melt pond, while the thick ice features are typically weathered first-year ridges.

To illustrate this variability, Figure 2-9 shows the ice thickness of three 100-m grids taken from the same floe in the Eastern Arctic [CRREL, unpublished data, Hanover, New Hampshire]. The grids were separated by several hundred meters. The figure implies that floes can be made of morphological regimes having totally different characteristics. For instance, Figure 2-9(a) shows thick very

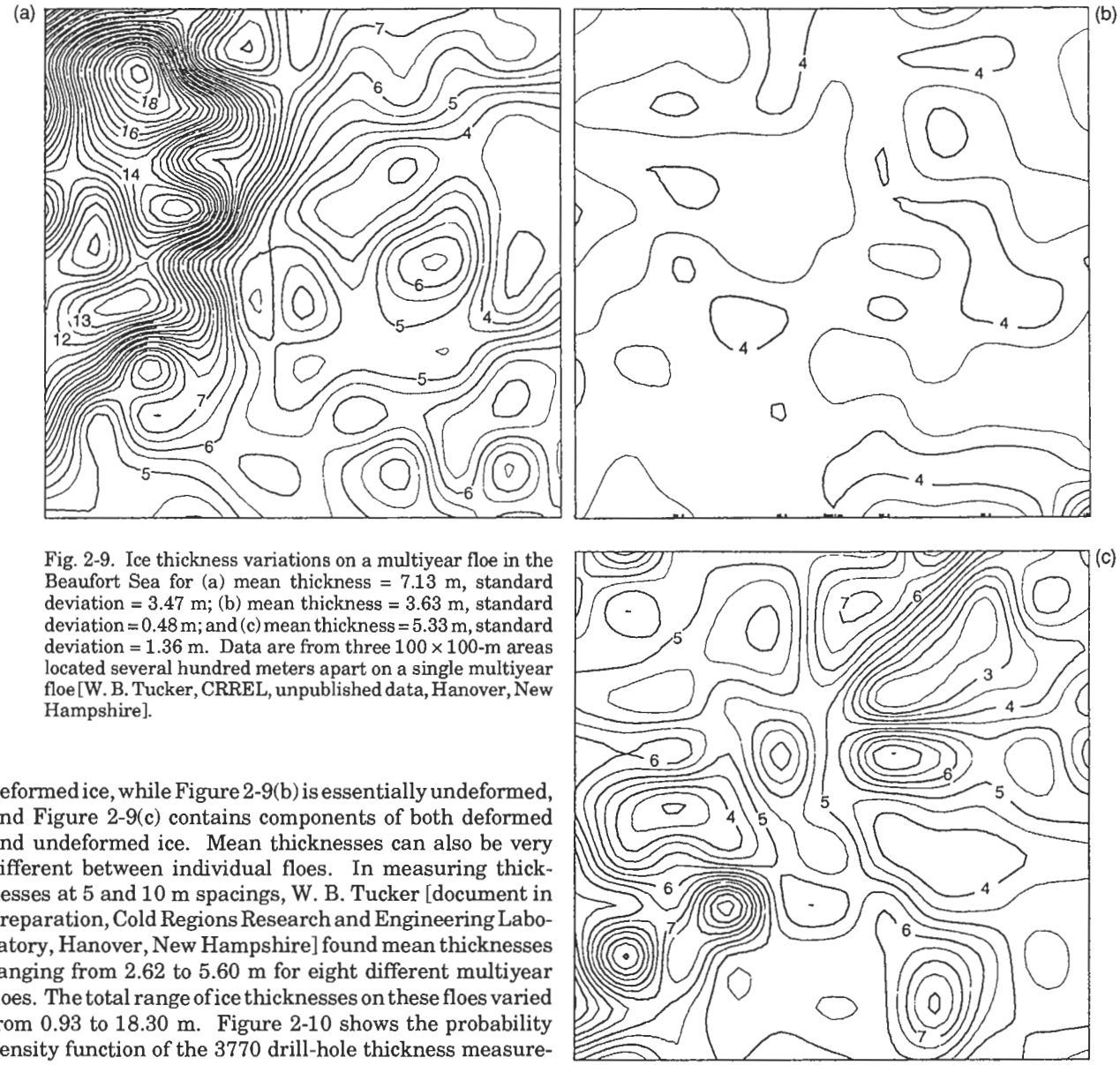

Fig. 2-9. Ice thickness variations on a multiyear floe in the Beaufort Sea for (a) mean thickness = 7.13 m, standard deviation = 3.47 m; (b) mean thickness = 3.63 m, standard deviation = 0.48 m; and (c) mean thickness = 5.33 m, standard deviation = 1.36 m. Data are from three 100 × 100-m areas located several hundred meters apart on a single multiyear floe [W. B. Tucker, CRREL, unpublished data, Hanover, New Hampshire].

deformed ice, while Figure 2-9(b) is essentially undeformed, and Figure 2-9(c) contains components of both deformed and undeformed ice. Mean thicknesses can also be very different between individual floes. In measuring thicknesses at 5 and 10 m spacings, W. B. Tucker [document in preparation, Cold Regions Research and Engineering Laboratory, Hanover, New Hampshire] found mean thicknesses ranging from 2.62 to 5.60 m for eight different multiyear floes. The total range of ice thicknesses on these floes varied from 0.93 to 18.30 m. Figure 2-10 shows the probability density function of the 3770 drill-hole thickness measurements made on these eight floes. The figure shows that the most likely multiyear ice thickness is 3.5 to 4.0 m, and also shows the long positive tail indicative of the presence of ridges.

The surface appearances of first-year and multiyear ice are quite different. Undeformed first-year ice is flat with little freeboard. When it has been deformed, the ridges consist of very distinct collections of angular blocks. Multiyear ice typically has a rolling hummocky appearance. Even undeformed multiyear floes have a surface relief of 10 to 20 cm as a result of differential melting. The undulating surface is easily identified from an aircraft if there is little snow cover. Multiyear ridges are distinct from first-year ridges because they are weathered and rounded, with little or no sign of the original block structure evident.

There are also major property differences in salinity, crystal texture, and porosity between first-year and multiyear ice. Figure 2-11 shows property profiles of multiyear and first-year ice sampled in early winter. Rather than porosity, the density is shown, but the differences in porosity are inherent in the density. The major differences are clarified by comparing these profiles. The salinity of first-year ice is considerably higher, particularly near the surface. For the upper 30 cm, first-year ice has a salinity of 6‰ to 7‰, while in the multiyear ice it is less than 1‰. For the remainder of the cores, salinities of first-year ice are consistently higher, except at the very bottom of the cores. First-year ice is characterized by well-defined platelet substructure in its crystal texture, whereas multiyear ice shows none. The grain boundaries in the upper 1.0 m of multiyear ice are not as sharp as those of first-year ice—a clear indication of crystal retexturing. Finally, the densi-

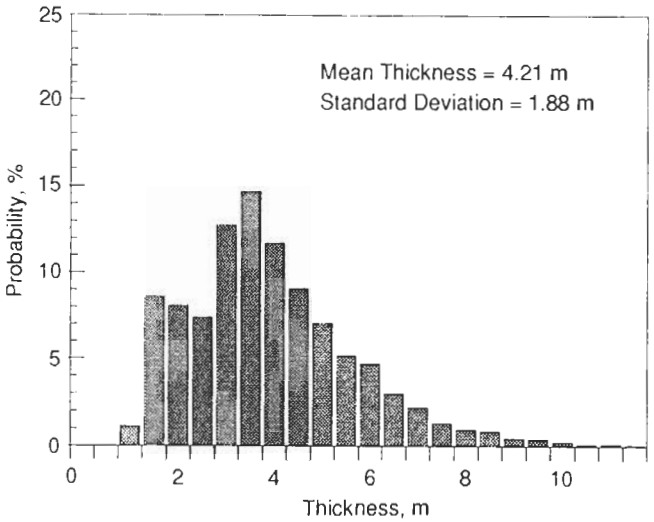

Fig. 2-10. Probability density function of 3770 ice thickness measurements made on eight Arctic multiyear floes.

ties of multiyear ice are lower than those of first-year ice in the upper layers. This reflects the increase in porosity due to the evacuation of brine inclusions and the enlargement of brine cavities and drainage channels during the melt season. Densities below 1.0 m are comparable in both cores.

A similar examination of the thickness and properties of first-year and multiyear ice in the Antarctic is instructive. Thickness variations are also found on Antarctic multiyear floes. For example, Eicken et al. [1991] found that the thickness of three cores spaced at 20 m on a single floe ranged from 1.27 to 2.15 m. A major difference from Arctic multiyear ice is that the thicknesses are considerably less due to the fact that ridges are much smaller than those found in the Arctic [Weeks et al., 1988]. Lange and Eicken [1991a] found a mean thickness of 1.53 m for apparently undeformed second-year ice and a mean thickness of 2.53 m for deformed second-year ice. However, Gow et al. [1987a] found thicknesses on different multiyear floes in the Weddell Sea ranging from 2.4 m to greater than 5.0 m. Many of the thicker floes showed no signs of having been deformed, indicating that thickness and the extent of deformation in

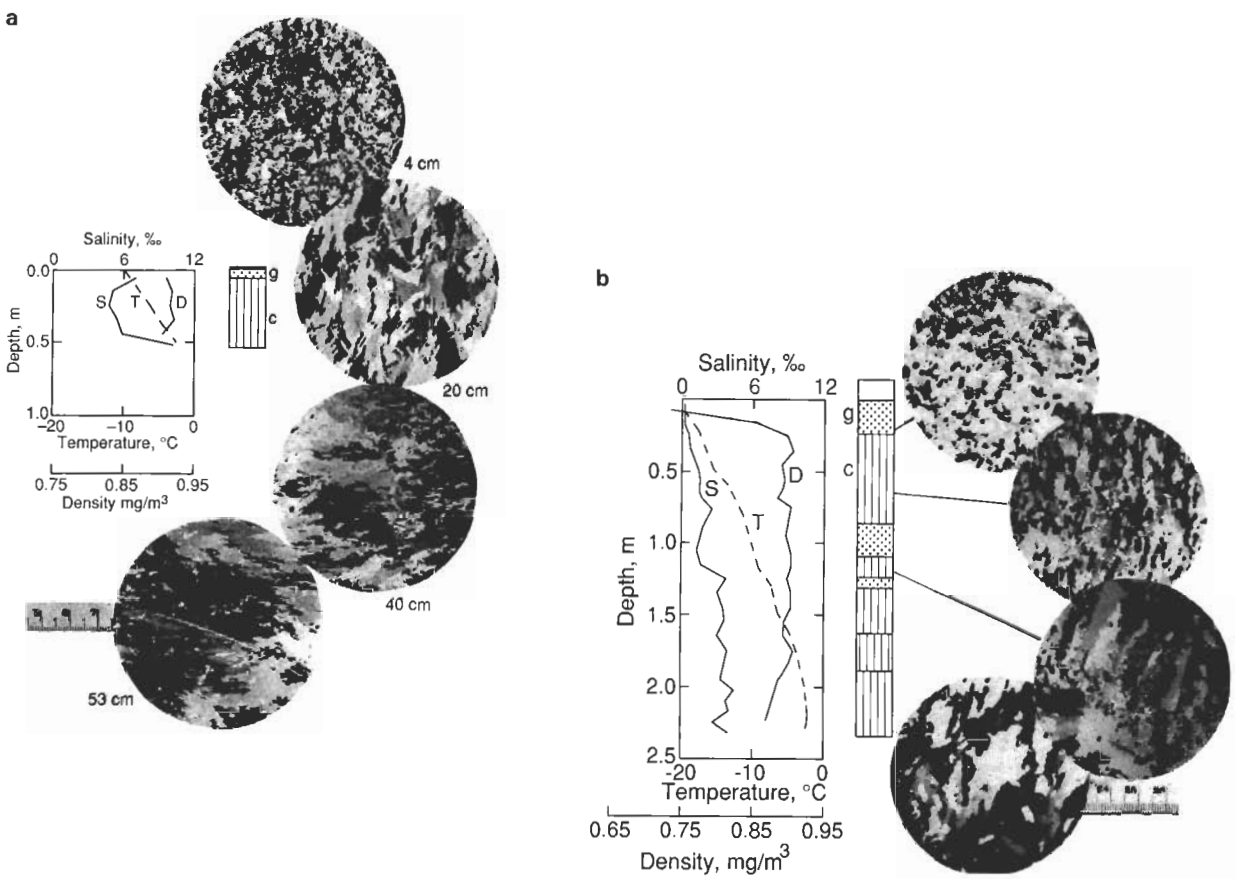

Fig. 2-11. Physical property and structure profiles of (a) lead ice 53 days after freeze-up [Gow et al., 1990] and (b) multiyear ice [CRREL, unpublished data, Hanover, New Hampshire].

the Weddell Sea pack ice can vary greatly with location in the pack.

Figure 2-12 shows core profiles of first-year and multiyear ice collected from the Weddell Sea, Antarctica. Only salinity and structural profiles were measured for these cores. The salinity profiles show that multiyear ice is somewhat less saline in the upper 40 cm. Below that, however, salinities of both ice types appear to hover around 4‰ to 5‰. The one exception to this is in the multiyear ice at a depth of 140 to 170 cm, where salinity falls to 2‰ to 3‰. This likely coincides with the transition from first- to second-year growth as evidenced by a change in the structure of the ice from congelation to frazil. It appears that frazil can be incorporated into the ice structure after the first year's growth as easily as during the first year. This implies that at least some frazil is forming in the water column beneath the existing ice sheet or being formed in leads and subsequently swept under adjacent ice [Lange and Eicken, 1991b]. Densities differ little between first-year and multiyear ice. Both the densities and the salinities indicate that minimal brine drainage and expansion of brine channels take place during the transformation of first- to second-year ice in the Weddell Sea.

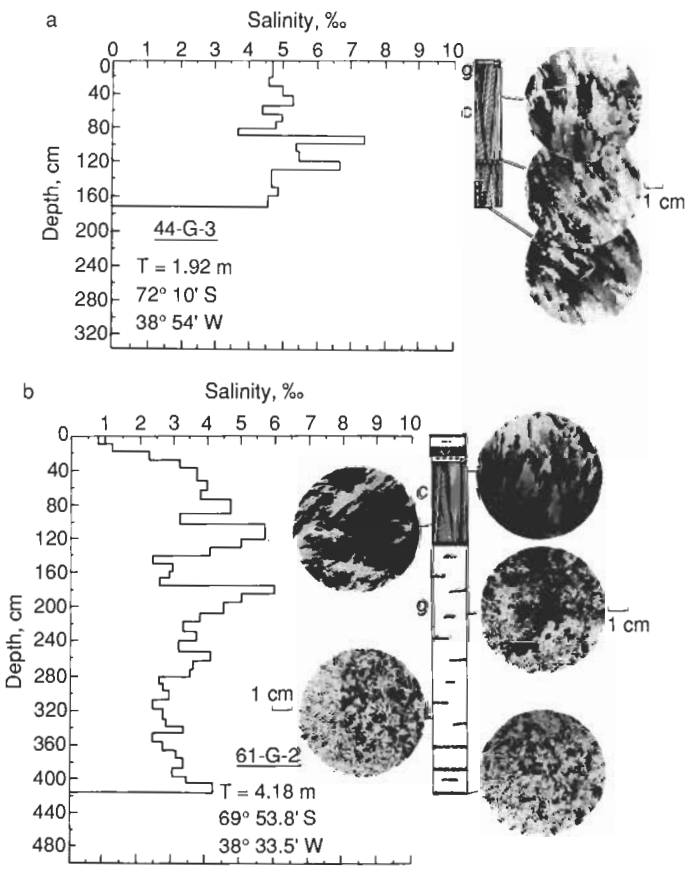

Fig. 2-12. Salinity and structure profiles of (a) first-year ice and (b) multiyear ice from the Weddell Sea, Antarctica. First-year ice consists of 94% congelation ice, whereas the multiyear ice is composed of 75% granular frazil formed during the second year of growth [Gow et al., 1987a].

Antarctic ice also exhibits large variations within a single floe. Examining the stratigraphy and salinities from closely spaced cores (with a separation of approximately 20 m) of two-year-old ice, Eicken et al. [1991] concluded that the variations in mean properties of cores taken within a few meters can vary as much as properties within an entire geographic region. Thicknesses of this relatively thin multiyear ice ranged from 1.27 to 1.54 m and the mean salinities varied from 4.1‰ to 7.0‰. The largest variability in the properties exists in the upper layers, which, as mentioned previously, are extremely important to microwave remote sensing. These variations appeared to be related to formation of the floe and deformation. Thus, it appears that large property variations can occur in Antarctic multiyear ice floes, although probably not to the extent observed in Arctic multiyear ice floes with their characteristic hummock–melt-pond morphology.

While we know that the variability of ice properties on multiyear ice is quite large, it has not been systematically quantified. It would be useful to conduct further surveys of properties on single multiyear floes to assist in quantifying these rather large property variations. This is particularly critical for the upper layers that most significantly affect microwave signatures. Knowledge is also needed of the range over which property variations occur relative to the size of the microwave footprint.

2.4 SURFACE PROPERTIES

Any discussion of remote sensing of sea ice would be incomplete without some attention being paid to the large variety of roughness features apparent on the surface of the ice cover. This is particularly important in the present context in that the surface roughness itself causes large variations in remote sensing signatures. Here we will dwell on roughness at two basic spatial scales. The first will be the large scale that we designate as that horizontal scale ranging from meters to kilometers and primarily includes features associated with deformation, although topography caused by melt ponds may be included. The other scale focuses on the small-scale roughness of the ice and snow surface ranging from millimeters to meters. There is a definite overlap between these two scales; for instance there are both small- and large-scale roughnesses associated with a brash ice field.

2.4.1 Deformation Features

Winds and currents keep the ice pack in nearly continuous motion, resulting in significant deformation of the ice cover. This can lead to the formation of a pack consisting of ice floes separated by water openings, which in itself is a roughness element since the freeboards of floes can vary from millimeters to several meters, as is the case of a ridge located on the edge of a floe. In the central pack, floes may be several kilometers in diameter. In the marginal ice zone

(MIZ), on the other hand, wave and wind action may thoroughly pulverize the ice, reducing floe sizes to less than a meter. Also characteristic of the MIZ and over large parts of the Antarctic is the formation of pancake ice.

Figure 2-13 shows small floes in the Labrador Sea MIZ incorporated into a brash ice field. Here the brash is made up of pulverized floes and newly forming frazil and is interspersed with broken blocks and floe pans.

Deformed ice constitutes a significant portion of the ice cover. Estimates made from submarine ice draft profiles indicate that the mass of ice contained in ridges is 25% to 50% of the total mass of ice in the Arctic [Wadhams, 1984; Williams et al., 1975]. Recent analysis of ice thickness measurements of Arctic multiyear floes [W. B. Tucker, document in preparation, CRREL, Hanover, New Hampshire] indicated that as much as 50% of multiyear ice may be deformed. That is, these floes contain a large component of ice that was deformed in its first-year state and that has subsequently aged and become incorporated into multiyear floes. Indeed, this deformed ice may be a major reason why that particular floe survived, having its thickness and strength increased by incorporation of the deformed ice.

The most notable roughness features caused by the deformation of sea ice are ridges and rubble fields. The ice sheet deforms under compression and shear, and blocks are piled both above and below the surface. Measurements of block sizes in a number of ridge sails [Tucker et al., 1984b] indicate that while most ridges are formed of ice less than 1-m thick, a considerable number are of thicker ice. Tucker et al. [1984b] also found a relationship between the ridge heights and the thickness of the ice contained within the ridges, which apparently results from the relation of ice strength to thickness. Freely floating ridges may have sails that exceed 10 m in height, while grounded ridges near shore can approach 20 m. Submarine ice draft measurements have found ridge keels extending to depths greater than 40 m [Wadhams, 1984].

Fig. 2-13. Incorporation of floe pans into a brash ice field in the Labrador Sea marginal ice zone during March 1989. (Photograph by M. R. Drinkwater.)

Ridges can be long linear features extending for several kilometers. More often, however, they are sinuous and extend for only several hundred meters. Repeated ridging causes rubble fields. Examples of typical Arctic first-year and multiyear ridges are shown in Figure 2-14. Because ridges are significant obstacles to surface transportation over pack ice, their statistics have been extensively studied. Surface ridge statistics have been obtained with airborne laser profilometers for many years [Wadhams, 1984; Hibler et al., 1974]. While estimating the mass of deformed ice from ridge counts extracted from laser terrain profiles may lead to errors [Rothrock, 1986], useful statistics on the surface roughness due to ridges can be obtained. Although much more information is available on ridging statistics in the Arctic than the Antarctic, Weeks et al. [1988] used the little available data to contrast ridging in various Arctic regions to that of the Ross Sea (Table 2-1). Lytle and Ackley [1991] found ridging in the Eastern Weddell Sea to be similar to that in the Ross Sea. Granberg and Leppäranta [1990], however, found evidence of increased ridging in the western sector of the Weddell Sea. These limited results, as well as impressions based on extensive visual observations, indicate that ridging is much more intense in the Arctic, with more and higher ridges than in the Antarctic. This difference presumably results from a less compact and less constrained pack being deformed in the Antarctic. Table 2-1 points out that near-coastal regions in both areas contain more ridges, a manifestation of the deformation occurring when the ice is forced towards the coast.

First-year ridges are composed of piles of very angular ice blocks. Voids between the blocks are frequently filled with wind-compacted snow. Tucker et al. [1984b] found that the sizes of the blocks generally scale linearly with the ice thickness, the largest dimension being about twice the thickness of the block. The sharp-edged blocks are ablated during summer to the point where there is little evidence of the original structure when the freezing season commences. Multiyear ridges are typically well rounded, hummocky features with few, if any, large voids. Their heights are also significantly less than first-year ridges. A typical multiyear ridge is shown in Figure 2-14(d). The porosities of the near-surface ice are high, while the brine volume is nearly zero, both resulting from the enhanced ablation and drainage occurring on the ridges during summer. There is a dearth of observations of multiyear ridges in the Antarctic. In the absence of surface melting, it is expected that these ridges would maintain their original blocky structure.

On a somewhat smaller roughness scale are broken ice fields and rafting. Frequently, sheets of thin ice are broken by wind, waves, or deformation, and the blocks often raft. When the water containing these blocks freezes, the newly formed sheet can have a vertical roughness ranging from a few centimeters up to a meter. Horizontal scales vary depending upon the original formation conditions, but can vary from centimeters to tens of meters. Rafting of ice sheets is a common occurrence. These may be long, linear,

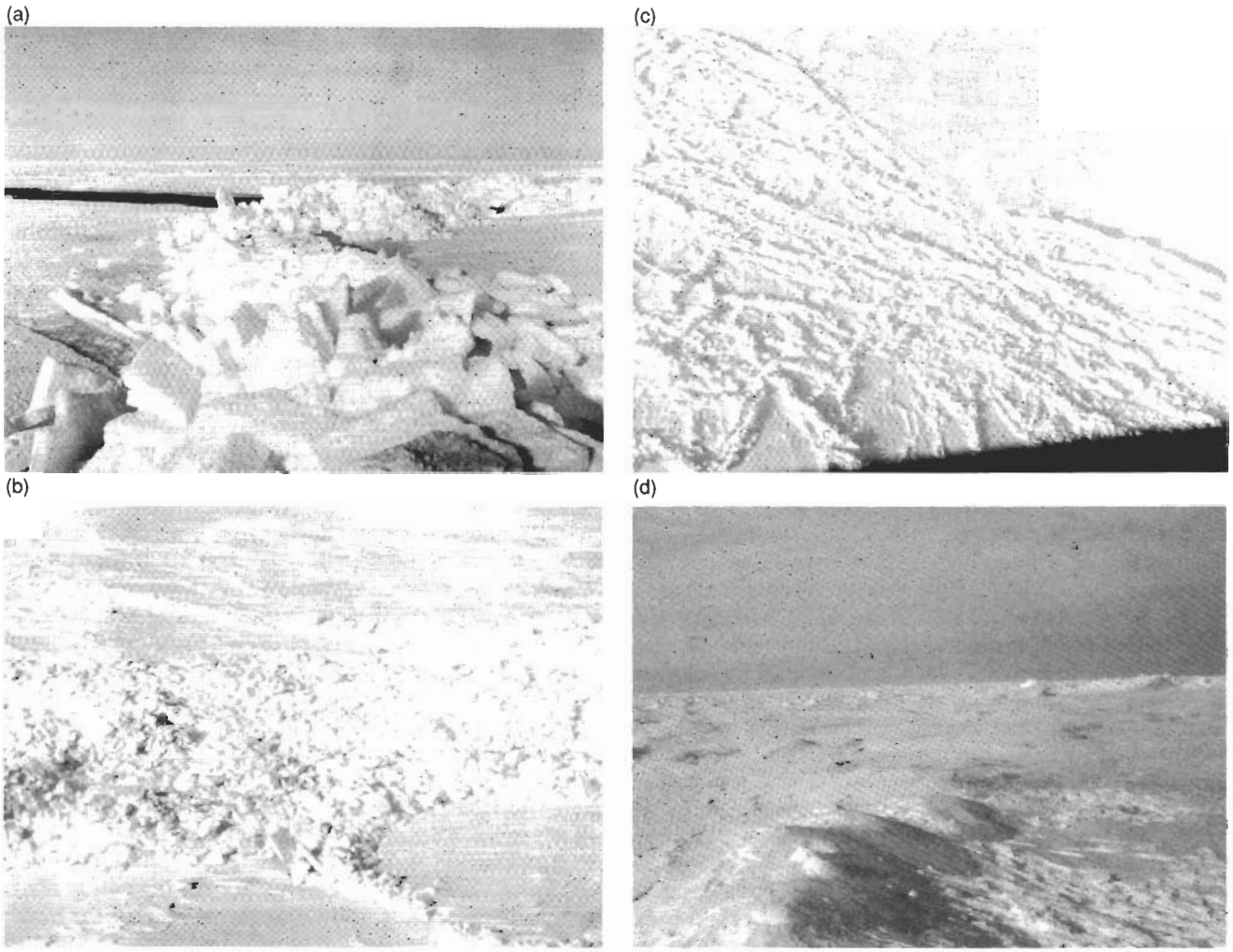

Fig. 2-14. Deformed ice: (a) free floating first-year ridge about 2 m in height; (b) grounded first-year ridge over 6 m in height; (c) aerial view of a 400-m-wide rubble field in the near-shore Beaufort Sea; and (d) multiyear ridge about 3 m in height.

Table 2-1. Ridging parameters from the Ross Sea compared to data from various Arctic locations for winter and early spring. Parameters were obtained from laser profilometer data from Weeks et al. [1988].

Location	Ridges per km	Mean ridge height, m
Ross Sea coastal	6.8	1.25
Ross Sea offshore	1.9	1.21
Central Beaufort Sea	2.6	1.47
Beaufort–Chukchi shear zone	4.4	1.51
West Eurasian Basin	4.7	1.50
North Greenland	8.2	1.68

or sinuous features extending several kilometers with vertical reliefs of less than a meter. Frequently, however, finger rafts occur, which have a distinctive square wave appearance. Like other rafts, horizontal and vertical dimensions are extremely variable.

While not a result of ice deformation, another mesoscale surface roughness feature is caused by the snow cover. The snow cover in both the Arctic and Antarctic is nonuniform, and significant topographic variations are created primarily by wind. Most noticeable are snow drifts, which, when compacted and hardened, are known as sastrugi. They are often associated with a morphological feature of the ice surface, such as an ice block, and they taper away from such a feature with the direction of the wind at the time they were created. These features are often several hundred meters in length with heights above the level surface of up to 1 m. Frequently observed on floes are rows of sastrugi, trending in the same general direction. Snow that drifts in around the bases of pressure ridges frequently reaches depths greater than 1 m.

2.4.2 *Small-Scale Surface Roughness*

Knowledge of the small-scale sea ice surface roughness is critical for the interpretation of microwave remote-sensing data. Over recent years, the development of a variety of instruments for this purpose has led to quantitative measurements of the roughness properties of a number of ice types. Most of these measurements have been made in the millimeter or centimeter range using profilometers employing either mechanical, photographic, or laser technology. Four principal methods are currently being used: (a) a mechanical roughness comb or rill meter [Drinkwater, 1989]; (b) a camera-based system with an automated digitizing and analysis system [Paterson et al., 1991]; (c) a tracked laser instrument for precise ranging along a meter baseline [Johansson, 1988; Farmer et al., 1991]; and (d) a manual method where a vertical slab is retrieved and photographed against a grid background [R. G. Onstott, personal communication, 1991].

Despite the numerous techniques, only a few measurements of small-scale ice roughness have been made. Drinkwater [1989] reported that the centimeter-scale roughness of first-year ice in the Labrador Sea may conform to either an exponential or Gaussian correlation function depending upon the degree of deformation of the surface. The surface was composed of flat ice pans separated by levees built from deformed brash ice or ridged blocks. The smooth ice had a standard deviation of 1.74 cm with a correlation length of 12.8 cm, while the standard deviation of the deformed ice was 4.43 cm and the correlation length was 18.6 cm. These measurements agree with those of Paterson et al. [1991], who found standard deviations of 0.78 and 5.26 cm for smooth and rough ice in the Labrador Sea. First-year ice in other Arctic areas appears to be smoother. This is probably because it has not been subjected to the harsher environment that characterizes the Labrador Sea MIZ. Kim et al. [1985] reported standard deviations of smooth and somewhat rougher ice to be 0.15 and 0.37 cm, presumably for samples from the Beaufort Sea. Likewise, in Chapter 5, R. G. Onstott reports a range of first-year ice roughnesses from 0.05 to 0.49 cm with correlation lengths of 0.5 to 3.7 cm for ice in the Eastern and Western Arctic. Farmer et al. [1991] also observed generally smaller roughnesses in the Beaufort Sea. They found standard deviations ranged from 0.18 to 0.40 cm and correlation lengths of 2.0 to 12.0 cm.

Observations of small-scale roughnesses of multiyear ice are sparse. Kim et al. [1985] reported standard deviations of 0.15 and 0.81 for smooth and rough multiyear ice, and correlation lengths of 8.2 and 8.9 cm, respectively. R. G. Onstott in Chapter 5 reports roughnesses of multiyear hummocks ranging from 0.26 to 0.89 cm, with correlation lengths of 2.8 to 6.0 cm. The standard deviations of frozen melt-pond surfaces were found to be much less, 0.08 to 0.21 cm. Correlation lengths ranged between 2.4 and 3.5 cm for these much smoother surfaces.

2.5 SNOW COVER

For much of the year, sea ice has another important surface feature—a snow cover. The areal extent and thickness of the snow cover is important for a number of reasons, particularly those concerning the thermodynamics of sea ice. During winter the snow acts as an insulating blanket, decreasing heat exchange with the ocean and retarding freezing, while in the summer the high albedo of the snow reduces the shortwave radiation input impeding surface melting [Maykut and Untersteiner, 1971]. How a snow cover impacts microwave signatures of sea ice and whether microwave data can be used to determine snow cover properties are important issues.

To date there has not been a large-scale effort to systematically measure the snow cover thickness on sea ice in the polar regions. However, there have been a few isolated studies. The results of these studies can be used to make several salient points regarding the temporal evolution of a snow cover, the geographical variability of snow depth, and the variations in snow depth between ice types. The thickness of the snow cover can exhibit tremendous variability, both temporally and spatially. Temporally, there are dramatic changes in snow cover during the summer melt cycle and the early snowfalls of fall freeze-up. In addition, there are the almost continual changes due to the wind redistributing the snow. On a large scale, very little is known regarding how snowfall varies within and between the different regions of the Arctic. On a small scale, snow depths are heavily influenced by ice surface topography and can vary from the bare ice of a frozen melt pond to a meter-thick snow cover in the lee of a pressure ridge over horizontal distances of only a few meters.

Field observations from the Central Arctic [Untersteiner, 1961] showed a steady increase in snow depth from August to October of about 0.15 m, followed by a gradual increase of 0.05 m until the onset of the melt season. Once melt began, the snow cover melted completely in only a few weeks. Based on a survey of prior measurements, Maykut and Untersteiner [1971] estimated a total snow depth of 0.40 m for ice in the Arctic Basin, 0.30 m of which was assumed to fall during September and October.

Table 2-2 summarizes snow survey results for three different regions in the Arctic. Each snow survey consisted of point measurements of snow depth made on a grid encompassing several thousand square meters. There is a large geographical disparity in mean snow depth with ice in the Greenland Sea MIZ having an average snow cover two and a half times as thick as the Eastern Arctic and three and a half times as thick as the Southern Beaufort Sea. Small-scale variations in snow depth are evident in the range of point measurements of snow depth, which vary from zero to over a meter.

Wadhams et al. [1987] made extensive measurements of snow depth on sea ice in the Weddell Sea. They found the mean snow depth to be quite variable with a general trend towards deeper snow at higher latitudes. The snow depth on a given floe depended primarily on the age of the floe and

Table 2-2. Summary of snow depths for Arctic multiyear ice. Beaufort Sea data are from W. B. Tucker [CRREL, unpublished data, Hanover, New Hampshire] and MIZ are from Perovich et al. [1988].

Location	Date	Latitude	Longitude	Number of points sampled	Mean	Standard deviation	Min. snow depth, cm	Max. snow depth, cm
Southern Beaufort Sea	April 1986	70° N	150° W	225	12.8	11.1	0	58
Eastern Arctic	November 1988	82° N	30° E	484	18.8	19.5	0	104
Greenland Sea MIZ	March 1987	78° N	2° W	570	46.5	24.1	3	120

on recent meteorological events, such as snowstorms and windstorms. Mean snow depths ranged from 0.00 to 0.40 m, with values typically falling between 0.10 and 0.15 m.

Studies in the Greenland Sea MIZ indicate that snow depth is significantly greater on multiyear ice than on first-year ice. Tucker et al. [1987] found that early summer snow depths on multiyear ice in the Greenland Sea MIZ ranged from 0.03 to 0.65 m, with an average of 0.28 m, while the snow on first-year ice never exceeded 0.20 m and averaged 0.08 m. Perovich et al. [1988] confirmed this during a winter experiment in the same region. They found a statistically significant difference in mean snow depth between multiyear floes (0.47 m) and first-year floes (0.11 m). As mentioned earlier, a heavy snow cover can impact the properties of the underlying sea ice by causing surface flooding with seawater.

The snow cover over Arctic sea ice is fairly simple. It consists primarily of wind-blown, hard-packed snow composed of well-rounded grains with diameters of 0.25 to 0.50 mm and a density between 0.3 and 0.4 mg/m^3. Ice layers, resulting from warm periods, are quite common in the snowpack. Occasionally, depth hoar can be found at the base of the snow cover. During most of the year the snow remains dry, usually having significant free water only during the summer melt period.

Frost flowers (Figure 2-15) can significantly impact the microwave remote-sensing properties of young ice [Drinkwater, 1988; Drinkwater and Crocker, 1988]. These flowers are formed by ice deposited on the surface directly from the vapor phase. The extent and form of the flowers depend primarily on the air temperature and level of supersaturation near the surface. Frost flower conditions can change rapidly, forming a dense mat in only a few hours and disappearing with only a small amount of surface flooding. In that frost flowers draw brine upwards from the new ice surface by capillary action as the freezing ice surface rejects brine, salinities as high as 110‰ have been measured in frost flowers [Drinkwater and Crocker, 1988]. The brine-enriched frost flowers form a rough dielectric interface in contrast to the smooth underlying ice surface. This interface strongly impacts the microwave signature and can lead to a misidentification of the ice type as discussed in later chapters.

The small-scale roughness of snow or frost flowers can also be important to microwave sensors. Unfortunately, there is a dearth of such measurements. Recent observations of the snow roughness on first-year ice in the Beaufort Sea found standard deviations to range from 0.18 to 0.40 cm, with correlation lengths of 2.0 to 12.0 cm [Farmer et al., 1991]. According to A. Carlström [personal communication, 1991], the mean root mean square roughness of young ice surfaces covered by frost flowers is 0.72 cm with a correlation length of 1.0 cm. These few measurements were obtained from the Beaufort Sea and the Central Arctic.

2.6 ICE PROPERTY STATISTICS

As interest in using microwave remote-sensing observations to monitor geophysical processes in sea ice has in-

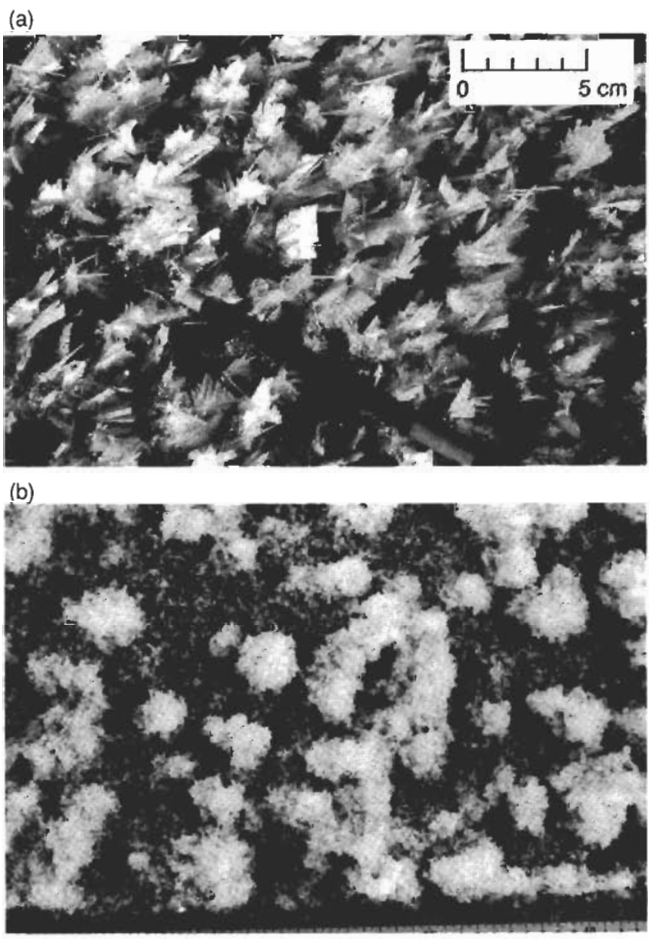

Fig. 2-15. Frost flowers: (a) enlarged view of individual frost flowers and (b) dense cover of clustered frost flowers on young sea ice.

creased, there has also been a growing awareness that in order to interpret these observations, an understanding is necessary of how variations in microwave signatures relate to differences in the physical properties and crystalline structure of the ice cover. To this point, only qualitative descriptions of the ice have been related to microwave signatures. Nonetheless, these characterizations, consisting of ice surface conditions and vertical profiles of ice crystal structure, temperature, salinity, brine volume, and density, have been shown to play a vital role in interpreting both passive and active microwave data [Arcone et al., 1986; Tucker et al., 1987, 1991].

However, for all their utility, such descriptive characterizations are insufficient for theoretical microwave models. Winebrenner et al. [1989] discussed the importance of a statistical description of ice structure for microwave modeling and have enumerated several useful statistical measures. Two such prominent microwave scattering models are the strong fluctuation theory [Tsang and Kong, 1981; Stogryn, 1984] and the dense medium radiative transfer model [Winebrenner et al., 1989].

The strong fluctuation theory requires characterization of the ice using the two-dimensional correlation function. Correlation functions for sea ice were investigated by Lin et al. [1988] in a combined experimental and theoretical effort. They analyzed a single horizontal thin-section photograph and found that the correlation function was exponential with correlation lengths comparable to the average size of the brine inclusions. Vallese and Kong [1981] examined correlation lengths for snow and determined that there was a correspondence to the average grain size of the snow.

The most extensive correlation function study for sea ice was performed by Perovich and Gow [1991] on saline ice grown in an outdoor pond. In this investigation, the correlation functions were determined for more than 50 thin-section photographs of this saline ice using a personal-computer-based image-processing system [Perovich and Hirai, 1988]. Figure 2-16 features a representative example of a correlation function for thin saline ice. A horizontal thin section was taken from the bottom of a 95-mm-thick ice sheet that had been growing for 48 hours, Figure 2-16(a). The ice was columnar with the *c*-axes of the component crystals being substantially horizontal. The sample was photographed at –10°C and had a salinity of 11‰, giving a brine volume of 6.1%. The two-dimensional correlation function, Figure 2-16(b), is peaked with a sharp drop-off, small regular sidelobes, and a shape that is more elliptical than circular. The correlation lengths in the major and minor directions are 0.15 and 0.12 mm, respectively, lengths that are closely associated with the physical size of the brine inclusions.

Perovich and Gow [1991] established that correlation lengths for young sea ice are directly related to physical features of the ice microstructure, such as the size of brine pockets in salty ice (typically tenths of a millimeter) and vapor inclusions in desalinated ice (typically millimeters). Like the ice microstructure, the correlation function of sea ice can be quite variable, depending on such parameters as

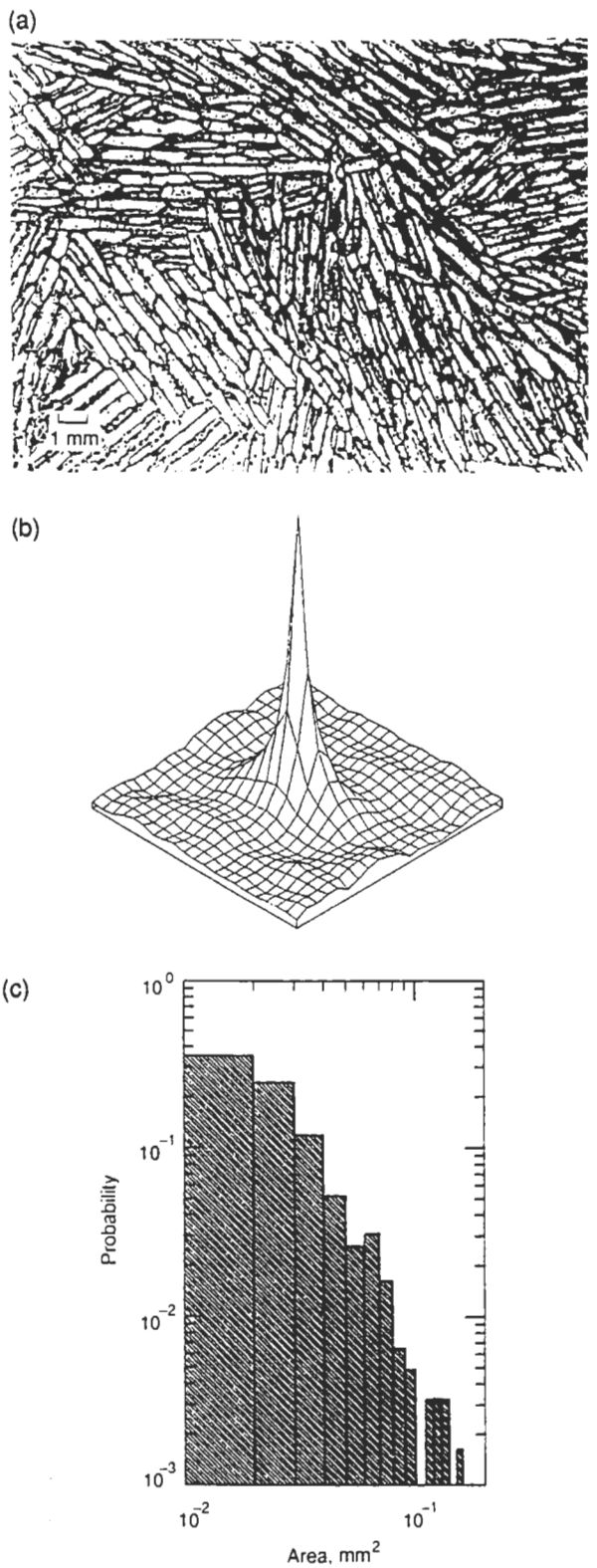

Fig. 2-16. Statistical descriptions of young sea ice microstructure: (a) horizontal thin section of young ice; (b) correlation function of this thin section; and (c) brine-pocket size distribution of the thin section [Perovich and Gow, 1991].

growth conditions, ice temperature, and brine volume. A growing ice sheet has the coldest temperatures at the surface and the warmest at the ice–water interface, with the brine volume increasing with depth. This produces a general trend of correlation lengths increasing with depth. They found that this trend can be overridden by structural changes in the ice microstructure, such as variations in the ice platelet diameter or a switch from columnar to granular crystals.

There are other possible statistical descriptors besides the correlation function. The brine pocket geometry and size distribution are important for the dense medium microwave models [Winebrenner et al., 1989]. Arcone et al. [1986] examined brine pocket geometry, using both horizontal and vertical thin sections of young columnar ice. They found that brine pockets were ellipsoidal with the long axis aligned within 15° of vertical. The vertical length of the brine pockets was typically 1 to 2 mm. In the horizontal, the major and minor axes of individual brine pockets varied considerably from 0.01 to 1.7 mm. A representative ratio of the three axes of the brine inclusion ellipsoids (length:major:minor) was 10:3:1.

As an example of brine pocket size distribution, Figure 2-16(c) shows the brine inclusion size distribution for the thin section presented in Figure 2-16(a). There were 615 inclusions in this 270 mm^2 section, with a total area of 17 mm^2 and a mean area of 0.028 mm^2. If we assume that the inclusions were elliptical with an aspect ratio of 0.8, similar to the correlation lengths for this thin section, then the mean values of the major and minor axes were 0.10 and 0.08 mm, respectively. These values are somewhat smaller but roughly comparable to the correlation lengths (0.15 and 0.12) calculated for this image. The brine-inclusion size distribution shows a sharp drop-off of probability (P) as the area (A) increases. This drop-off is well fit ($R^2 = 0.96$) by a power law with $P = 1.9 \times 10^{-5} A^{-2.5}$.

2.7 SUMMARY

In this chapter, we have attempted to illuminate aspects of sea ice that are believed to affect microwave remote sensing. In doing so, it was necessary to delve in some detail into certain processes, such as ice growth and its dynamic and thermal modifications. This was done primarily to provide a brief background useful in understanding the state of the ice at various stages in its history.

Although the physical properties of sea ice have been studied for many years, they have recently taken on new significance due largely to increased remote sensing of the polar regions. While the emphasis has been to characterize and understand properties important to remote sensing, the increased attention to ice properties has enabled us to better understand properties and processes in their own right. This process is expected to continue as sensors are continually refined.

There is a need to provide better quantification of properties. This process has begun as described in the last section and will continue under the guidance of the needs of microwave models. Techniques of quantitatively describing small- and large-scale properties, both in vertical and horizontal dimensions, will be necessary to provide input to microwave models. Coupled with quantification of properties will be the need to model the ice properties themselves. One possibility is to develop empirical models to predict the temporal evolution of ice properties. As our understanding of complex processes increases, the models can become more physically based, and should aim to predict the spatial and temporal evolution of properties from climatic or thermodynamic input. Needless to say, ice properties and processes must continue to be studied in laboratory and field experiments to enhance the theoretical development of process models, which in turn can provide a firm base for microwave models.

REFERENCES

Ackley, S., On the differences in ablation seasons of the Arctic and Antarctic sea ice, *Journal of Atmospheric Science, 39(3),* pp. 440–447, 1982.

Andreas, E. L. and S. F. Ackley, On the differences in ablation seasons of the Arctic and Antarctic sea ice, *Journal of Atmospheric Science, 39(3),* pp. 440–447, 1982.

Arcone, S. A., A. J. Gow, and S. McGrew, Structure and dielectric properties at 4.8 and 9.5 GHz of saline ice, *Journal of Geophysical Research, 91,* pp. 14,281–14,303, 1986.

Bilello, M. A., Decay patterns of fast sea ice in Canada and Alaska, *Sea Ice Processes and Models,* edited by R. S. Pritchard, pp. 313–326, University of Washington Press, Seattle, Washington, 1980.

Campbell, K. J. and A. S. Orange, The electrical anisotropy of sea ice in the horizontal plane, *Journal of Geophysical Research, 79,* pp. 5059–5063, 1974.

Carsey, F. D., S. A. Digby, S. Argus, M. J. Collins, B. Holt, C. E. Livingstone, and C. L. Tang, Overview of LIMEX'87 ice observations, *IEEE Transactions on Geoscience and Remote Sensing, 27(5),* pp. 468–484, 1989.

Cherepanov, N. V., Spatial arrangement of sea ice crystal structure, *Problemy Arktiki i Antarktiki, 38,* pp. 176–181, 1971.

Colony, R. and A. S. Thorndike, Sea ice motion as a drunkard's walk, *Journal of Geophysical Research, 90,* pp. 965–974, 1985.

Comiso, J. C., Arctic multiyear ice classification and summer ice cover using passive microwave satellite data, *Journal of Geophysical Research, 95(C8),* pp. 13,411–13,422, 1990.

Cox, G. F. and W. F. Weeks, *Brine Drainage and Initial Salt Entrapment in Sodium Chloride Ice,* CRREL Research Report 345, 85 pp., Cold Regions Research and Engineering Laboratory, Hanover, New Hampshire, 1975.

Cox, G. F. N. and W. F. Weeks, Numerical simulations of the profile properties of undeformed first-year sea ice during the growth season, *Journal of Geophysical Research, 93,* pp. 12,449–12,460, 1988.

Dieckmann, G., G. Rohardt, H. Hellimer, and J. Kipfstul, The occurrence of ice platelets at 250-m depth near the Filchner Ice Shelf and its significance for sea ice biology, *Deep Sea Research, 33,* pp. 141–148, 1986.

Doronin, Y. P. and D. E. Kheisin, *Sea Ice,* 323 pp., Girdrometeoizdat Publishers, Leningrad, 1975 (NSF Trans. TT75-52088, 1977).

Drinkwater, M. R., Important changes in microwave scattering properties of young snow-covered sea ice as indicated from dielectric modeling, *Proceedings of the 1988 International Geoscience and Remote Sensing Symposium (IGARSS'88),* pp. 793–797, University of Edinburgh, Edinburgh, UK, 1988.

Drinkwater, M. R., LIMEX'87 ice surface characteristics; implications for C-band SAR backscatter signatures, *IEEE Transactions on Geoscience and Remote Sensing, 27(5),* pp. 501–513, 1989.

Drinkwater, M. R. and G. B. Crocker, Modelling changes in the dielectric and scattering properties of young snow-covered sea ice at GHz frequencies, *Journal of Glaciology, 34(118),* pp. 274–282, 1988.

Drinkwater, M. R. and V. A. Squire, C-band SAR observations of marginal ice zone rheology in the Labrador Sea, *IEEE Transactions on Geoscience and Remote Sensing, GE-27,* pp. 522–534, 1989.

Eicken, H., M. A. Lange, and G. S. Dieckmann, Spatial variability of sea-ice properties in the Northwestern Weddell Sea, *Journal of Geophysical Research, 96,* pp. 10,603–10,615, 1991.

Eide, L. I. and S. Martin, The formation of brine drainage features in young sea ice, *Journal of Glaciology, 14,* pp. 137–154, 1975.

Farmer, L. D., M. R. Drinkwater, T. I. Lukowski, L. D. Arsenault, C. E. Livingstone, A. Kovacs, D. L. Bell, F. Fetterer, S. A. Digby–Carsey, L. M. H. Ulander, A. Carlström, W. Stringer, and L. Shapiro, *Beaufort Sea Ice—1, Field Data Report,* 102 pp., Naval Oceanographic and Atmospheric Research Laboratory, Branch Office, Hanover, New Hampshire, 1991.

Gow, A. J., Orientation textures in ice sheets of quietly frozen lakes, *Journal of Crystal Growth, 74,* pp. 247–258, 1986.

Gow, A. J. and W. B. Tucker III, Sea ice in the polar regions, *Polar Oceanography, Part A: Physical Science,* edited by Walker O. Smith, pp. 47–122, Academic Press, San Diego, California, 1990.

Gow, A. J., S. F. Ackley, W. F. Weeks, and J. W. Govoni, Physical and structural characteristics of Antarctic sea ice, *Annals of Glaciology, 3,* pp. 113–117, 1982.

Gow, A. F., S. F. Ackley, K. R. Buck, and K. M. Golden, *Physical and Structural Characteristics of Weddell Sea Pack Ice,* CRREL Report 87-14, 70 pp., Cold Regions Research and Engineering Laboratory, Hanover, New Hampshire, 1987a.

Gow, A. J., W. B. Tucker, and W. F. Weeks, *Physical Properties of Summer Sea Ice in the Fram Strait, June–July,* CRREL Report 87-16, 81 pp., Cold Regions Research and Engineering Laboratory, Hanover, New Hampshire, 1987b.

Gow, A. J., D. A. Meese, D. K. Perovich, and W. B. Tucker III, The anatomy of a freezing lead, *Journal of Geophysical Research, 95,* pp. 18,221–18,232, 1990.

Granberg, H. B. and M. Leppäranta, *Helicopter-Borne Remote Sensing of Antarctic Sea Ice Using a Laser Profiler, Synchronized Video and 70 mm Camera During Finnarp-89,* paper presented at International Association for Hydraulic Research (IAHR) Ice Symposium 1990, IAHR, Espoo, Finland, 1990.

Hibler, W. D., A. J. Mock, and W. B. Tucker, Classification and variation of sea ice in the western Arctic Basin, *Journal of Geophysical Research, 79,* pp. 2735–2743, 1974.

Johansson, R., *Laser-Based Surface Roughness Measurements of Snow and Sea Ice on the Centimeter Scale,* Research Report 162, 34 pp., Department of Radio and Space Science, Chalmers University of Technology, Göteborg, Sweden, 1988.

Kim, Y. S., R. K. Moore, R. G. Onstott, and S. Gogineni, Towards identification of optimum radar parameters for sea ice monitoring, *Journal of Glaciology, 31(109),* pp. 214–219, 1985.

Koerner, R. M., The mass balance of sea ice of the Arctic Ocean, *Journal of Glaciology, 12,* pp. 173–185, 1973.

Kovacs, A. and R. Morey, Radar anisotropy of sea ice due to preferred azimuthal orientation of the horizontal *c*-axes of ice crystals, *Journal of Geophysical Research, 83,* pp. 6037–6046, 1978.

Lake, R. A. and E. L. Lewis, Salt rejection by sea ice during growth, *Journal of Geophysical Research, 75(30),* pp. 583–597, 1970.

Lange, M. A. and H. Eicken, The sea ice thickness distribution in the Northwestern Weddell Sea, *Journal of Geophysical Research, 96,* pp. 4821–4837, 1991a.

Lange, M. A. and H. Eicken, Texture characteristics of sea ice and the major mechanisms of ice growth in the Weddell Sea, *Annals of Glaciology, 15,* pp. 210–215, 1991b.

Lange, M. A., S. F. Ackley, P. Wadhams, G. S. Dieckmann, and H. Eicken, Development of sea ice in the Weddell Sea, Antarctica, *Annals of Glaciology, 12,* pp. 92–96, 1989.

Lange, M. A., P. Schlosser, S. F. Ackley, P. Wadhams, and G. S. Dieckmann, O^{18} concentrations in the sea ice of the Weddell Sea, Antarctica, *Journal of Glaciology, 36,* pp. 315–323, 1990.

Langhorne, P. J., Laboratory experiments on crystal orientation in NaCl ice, *Annals of Glaciology, 4,* pp. 163–169, 1983.

Langhorne, P. J. and W. H. Robinson, Alignment of crystals in sea ice due to fluid motion, *Cold Regions Science and Technology, 12,* pp. 197–214, 1986.

Lin, F. C., J. A. Kong, R. T. Shin, A. J. Gow, and S. A. Arcone, Correlation function study for sea ice, *Journal of Geophysical Research, 93,* pp. 14,055–14,063, 1988.

Lofgren, G. and W. F. Weeks, Effect of growth parameters on substructure spacing in NaCl ice crystals, *Journal of Glaciology, 7,* pp. 153–163, 1969.

Lytle, V. I. and S. F. Ackley, Sea ice ridging in the Eastern Weddell Sea, *Journal of Geophysical Research, 96(10),* pp. 18,411–18,416, 1991.

Martin, S., A field study of brine drainage and oil entrainment in first-year sea ice, *Journal of Glaciology, 22,* pp. 473–502, 1979.

Maykut, G. A., The ice environment, *Sea Ice Biota,* edited by R. A. Horner, pp. 21–82, CRC Press, Boca Raton, Florida, 1985.

Maykut, G. A. and N. Untersteiner, Some results from a time-dependent thermodynamic model of sea ice, *Journal of Geophysical Research, 76,* pp. 1550–1575, 1971.

Nakawo, M. and N. K. Sinha, A note on the brine layer spacing of first-year sea ice, *Atmosphere–Ocean, 22(2),* pp. 193–206, 1984.

Neumann, G. and W. J. Pierson, Jr., *Principles of Physical Oceanography,* 545 pp., Prentice–Hall, Englewood Cliffs, New Jersey, 1966.

Paige, R. A., *Crystallographic Studies of Sea Ice in McMurdo Sound, Antarctica,* Technical Report R494, 31 pp., Naval Civil Engineering Laboratory, Port Hueneme, California, 1966.

Paterson, J. S., B. Brisco, S. Argus, and G. Jones, In-situ measurements of micro-scale surface roughness of sea ice, *Arctic, 44(1), Supplement 1,* pp. 140–146, 1991.

Perovich, D. K. and A. J. Gow, A statistical description of the microstructure of young sea ice, *Journal of Geophysical Research, 96,* pp. 16,943–16,953, 1991.

Perovich, D. K. and A. Hirai, Microcomputer-based image-processing systems, *Journal of Glaciology, 34,* pp. 249–252, 1988.

Perovich, D. K., A. J. Gow, and W. B. Tucker III, Physical properties of snow and ice in the winter marginal ice zone of Fram Strait, *Proceedings of the IGARSS'88 Symposium,* pp. 1119–1123, Edinburgh, Scotland, ESA SP-284, European Space Agency, Noordwijk, Netherlands, 1988.

Rothrock, D. A., Ice thickness distribution—measurement and theory, *The Geophysics of Sea Ice,* edited by N. Untersteiner, pp. 551–575, NATO ASI Series B: Physics vol. 146, Plenum Press, New York, 1986.

Stander, E. and B. Michel, The effects of fluid flow on the development of preferred orientations in sea ice: laboratory experiments, *Cold Regions Science and Technology, 17,* pp. 153–161, 1989.

Stogryn, A., Correlation functions for random granular media in strong fluctuation theory, *IEEE Transactions on Geoscience and Remote Sensing, GE-22,* pp. 150–154, 1984.

Tsang, L. and J. A. Kong, Scattering of electromagnetic waves from random media with strong permittivity fluctuations, *Radio Science, 16,* pp. 303–320, 1981.

Tucker, W. B., A. J. Gow, and J. A. Richter, On small-scale variations of salinity in first-year sea ice, *Journal of Geophysical Research, 89,* pp. 6505–6514, 1984a.

Tucker, W. B., D. S. Sodhi, and J. W. Govoni, Structure of first-year pressure ridge sails in the Alaskan Beaufort Sea, *The Alaskan Beaufort Sea: Ecosystems and Environment,* edited by P. W. Barnes et al., pp. 115–135, Academic Press, New York, 1984b.

Tucker, W. B., III, A. J. Gow, and W. F. Weeks, Physical properties of summer sea ice in Fram Strait, *Journal of Geophysical Research, 92(C7),* pp. 6787–6803, 1987.

Tucker, W. B., III, T. C. Grenfell, R. G. Onstott, D. K. Perovich, A. J. Gow, R. A. Shuchman, and L. L. Sutherland, Microwave and physical properties of sea ice in the winter marginal ice zone, *Journal of Geophysical Research, 96,* pp. 4573–4587, 1991.

Untersteiner, N., On the mass and heat budget of the Arctic sea ice, *Archiv fuer Meteorologie, Geophysik, und Bioklimatologie, A(12),* pp. 151–182, 1961.

Vallese, F. and J. A. Kong, Correlation function studies for snow and ice, *Journal of Applied Physics, 52,* pp. 4921–4925, 1981.

Wadhams, P., Sea ice morphology and its measurement, *Arctic Technology and Policy,* edited by I. Dyer and C. Chryssostomidis, pp. 179–195, Hemisphere Publishing Corporation, Washington, DC, 1984.

Wadhams, P., M. A. Lange, and S. F. Ackley, The ice thickness distribution across the Atlantic section of the Antarctic Ocean in midwinter, *Journal of Geophysical Research, 92(C13),* pp. 14,535–14,552, 1987.

Weeks, W. F. and S. F. Ackley, The growth, structure and properties of sea ice, *The Geophysics of Sea Ice,* edited by N. Untersteiner, pp. 9–164, NATO ASI Series B: Physics vol. 146, Plenum Press, New York, 1986.

Weeks, W. F. and A. J. Gow, Preferred crystal orientations in the fast ice along the margins of the Arctic Ocean, *Journal of Geophysical Research, 83,* pp. 5105–5121, 1978.

Weeks, W. F. and A. J. Gow, Crystal alignments in the fast ice of Arctic Alaska, *Journal of Geophysical Research, 85,* pp. 1137–1146, 1980.

Weeks, W. F. and W. L. Hamilton, Petrographic characteristics of young sea ice, Point Barrow, Alaska, *American Mineralogy, 47,* pp. 945–961, 1962.

Weeks, W. F. and O. S. Lee, The salinity distribution in young sea ice, *Arctic, 15,* pp. 92–108, 1962.

Weeks, W. F. and G. Lofgren, The effective solute distribution during the freezing of NaCl solutions, *Proceedings of the International Conference on Low Temperature Science, Physics of Snow and Ice, I(1),* pp. 579–597, edited by H. Oura, Institute of Low Temperature Science, Hokkaido University, Sapporo, Japan, 1967.

Weeks, W. F., S. F. Ackley, and J. W. Govoni, Sea ice ridging in the Ross Sea, Antarctica, as compared with sites in the Arctic, *Journal of Geophysical Research, 94,* pp. 4984–4988, 1988.

Williams, E., C. W. M. Swithinbank, and G. deQ Robin, A submarine study of Arctic pack ice, *Journal of Glaciology, 15,* pp. 349–362, 1975.

Winebrenner, D. P., L. Tsang, B. Wen, and R. West, Sea ice characterization measurements needed for testing of microwave remote sensing models, *IEEE Journal of Oceanic Engineering, 14(2),* pp. 149–158, 1989.